AD 636593

ANNUAL PROGRESS REPORT

JUNE 1966

ATMOSPHERIC PHYSICS

School of Physics

D D C
RECEIVED
AUG 11 1966
C

CLEARINGHOUSE
FOR FEDERAL SCIENTIFIC AND
TECHNICAL INFORMATION

Hardcopy	Microfiche		
$3.00	$ .50	57 pp	

ARCHIVE COPY

UNIVERSITY OF MINNESOTA

ANNUAL PROGRESS REPORT

JUNE 1966

AP-24

Contract Number Nonr-710(22)

ATMOSPHERIC PHYSICS RESEARCH

University of Minnesota
Minneapolis, Minnesota

PREFACE

This report summarizes the research performed under Contract Nonr-710(22) for the year ending 31 May 1966. The work is in various stages of completion as reflected by the differing format of the four reports covering the various areas of research.

The first two papers of this report are essentially scientific reports representing the culmination of one phase of the research. The last two papers are more in the nature of status reports on current research. A final note on stellar scintillation has been appended simply to indicate continuing interest in this field although the demands made on experimenters' time on other projects precluded further work on this area during the past year.

TABLE OF CONTENTS

Page

An Experimental Study of the Equation of Motion in the Free Atmosphere by Homer T. Mantis ---------- 1

The Vertical Distribution of Dust by James M. Rosen ---------- 37

Solar Extinction by F. C. Gillett and T. J. Pepin ---------- 42

Dust Collection from the Stratosphere by James M. Rosen ---------- 45

Stellar Extinction and Scintillation ---------- 51

An Experimental Study of the Equation

of Motion in the Free Atmosphere

by

Homer T. Mantis

1. Introduction

The energy of atmospheric motions is distributed over a sufficiently broad band of frequencies or scales that a quantitative application of the conservation laws of mechanics to a specific frequency domain may still present difficulty. The conventional formulation of the equation of motion as applied to the weather map, for example, which may be written

$$\frac{d\vec{V}}{dt} + f\,\vec{k} \times \vec{V} = -g\,\nabla p\,h + \vec{F}_r \qquad (1)$$

is based on Reynold's hypothesis that it is possible to define the velocity, accelerations and forces on a uniform scale (Miller, 1951). The frictional force F_r in this equation represents a transfer of momentum from weather map or synoptic scale by motions of lesser scale.

Difficulties with the application of Eq. (1) may be appreciated by noting that in the free atmosphere it has not been possible to use the equation even as a phenomenological definition of the frictional force by a computation of a difference in the forces and the accelerations. The problem is largely that of smoothing the fields of wind and pressure on the same scale and, in practice, is caused almost in equal measure by the ill defined error of measurement and incomplete specification of the wind and pressure by the present network of meteorological observations.

This paper presents the results of an experimental study to determine the representative magnitudes of the various terms of Eq. (1) as applied to motions of synoptic scale in the free atmosphere, specifically at the 500 mb and 300 mb levels. For the reasons detailed above, it was necessary to attack the problem

obliquely by a statistical analysis of data derived by objective procedures. As in most statistical studies, the representative magnitude of a quantity is assumed to be specified by its mean and variance. In this sense, it has been possible to estimate the magnitude of the following quantities of meteorological interest:

a) The atmospheric accelerations at synoptic scale.

b) The frictional force at synoptic scale (actually, evidence is presented simply to the effect that the frictional force must have the same magnitude as the synoptic acceleration).

c) The synoptic scale departure of the wind from geostrophic equilibrium (the sum of (a) and (b)).

d) The smaller scale structure of the wind observed by the conventional radiosonde.

There are, as well, a number of interesting by-products of this investigation. In the course of the study, statistics on the magnitude of the first and second horizontal derivatives of the field of isobaric height were computed. These results should be useful as a climatological guide in constructing or testing models of large scale atmospheric flow. The poleward transport of momentum was found to occur in a systematic pattern of accelerations, a result which has such broad implications for models of the general circulation, it is discussed in a separate section of this report.

2. Radionale for the definition of synoptic scale.

The spacing of upper air observing stations ultimately will set a limit to the horizontal dimensions of systems which can be represented on the weather map. Although the spacing of upper air observing stations is irregular, the typical spacing in continental United States is from 250 to 350 km. The present network appears capable of delineating systems with horizontal dimensions in

excess of 1000 km, an arbitrary figure which is often used as the limit of synoptic scale. Even an isolated jet stream which has a transverse dimension of 500 km (e.g. Endlich and McLean, 1965) would fall within this definition of synoptic scale.

Primarily due to studies made by Buell (1957, 1958, 1960), it is known that the typical dimensions of upper air systems in the pressure field (the pressure field determined from the radiosonde observation and the hydrostatic computation of pressure height) are greater than 2000 km and only a small fraction of the variance of isobaric height can be associated with systems of smaller scale. Studies of wind structure show that the variance of the radiosonde wind must be distributed over a wider range of scales (Eddy, 1964) although the spectral analysis of a vector quantity requires more information than a scaler variable and details of the wind structure are lacking.

As the subsequent analysis will show, the variance of isobaric height is so nearly restricted to larger scale systems, the analysis of the pressure gradient force at synoptic scale requires little smoothing or filtering; the problem is really one of interpolation with only a minimal amount of smoothing. The horizontal contour gradients were derived by a process of numerical interpolation and smoothed to eliminate systems smaller than 1000 km. The pressure gradient force determined in this way conveniently defines the synoptic scale pressure systems. The wind field was not smoothed on this same scale. Instead, a comparison of the force and wind field was accomplished by interpolating the contour gradients at the location of a radiosonde wind observation. The scale analysis of the wind field was then made by comparing the dimensions of the wind system to the dimensions of the synoptic scale pressure field.

3. The numerical interpolation of the pressure gradient force.

In contrast to the conventional meteorological analysis of the field of isobaric height which is used to interpolate a value of the height at fixed grid points, the purpose of this analysis is to interpolate (as it finally developed) all the first and second order horizontal derivatives, five derivatives in all, at a point where a wind observation is made. The irregularity of station spacing as well as observational error and small scale variability make it necessary to interpolate the derivatives from a larger set of observations than the minimum required to specify five derivatives. After some experimentation with interpolation polynomials of various degree including the third, a weighted polynomial of second degree fitted to ten observations of isobaric height was used in this study. Symbolically, coefficients of the polynomial

$$h_p = A_1 x^2 + A_2 x y + A_3 y^2 + A_4 x + A_5 y + A_6 \qquad (2)$$

were calculated for each observing period by minimizing the expression

$$\sum_{i=1}^{10} (h_{oi} - h_{pi})^2 \left(\exp - \frac{r_i^2}{R^2}\right) .$$

The quantity h_{oi} is the isobaric height observed at the ith station and h_{pi} the height at that station predicted by the interpolation polynomial. The origin of the polynomial was located at the point for which the derivatives are to be interpolated and the exponent of the error type weighting function is the square of the distance from the observation to the point of interpolation[1], $r_i^2 = x_i^2 + y_i^2$. The weighting scale parameter R was set to equal

1. The position of the observing stations were calculated in a Cartesian coordinate system with the axis located on the central observing station of the given net. So that the analysis could be readily compared with conventional meteorological charts, the calculation was performed using a mathematical specification of a Lambert Conformal Conic projection with standard parallels at 30° and 60° latitude. The station location was entered to the nearest minute of latitude and longitude according to the Weather Bureau publication, Key to Meteorological Records Documentation No. 5.21, History and Catalogue of Upper Air Data for the Period 1946-1960, (1964).

500 km. The least square fit with this weighting factor has the effect of placing primary weight on the four or five observations lying with a radius of 500 km and of also smoothing the derivatives, primarily the second derivatives, on a scale of approximately 1000 km.

The second degree polynomial has frequently been used in objective weather map analysis, most recently by Corby (1961). It is worthy of reiteration, however, that in almost every instance, the coefficient A_6 in (2) is the value interpolated. In the present analysis, the coefficients A_1 through A_5 are the end product of the interpolation scheme.

Coefficients A_4 and A_5 are, of course, proportional to the components of the horizontal pressure gradient force. If the coordinates of the polynomial are rotated so that the x' axis is aligned with the grostrophic wind, the first three coefficients are proportional to the second derivatives and will have, as well, a meteorological interpretation that is readily recognized. The coefficients in the rotated system are indicated with a prime. With the appropriate scaling factors, they will have the following interpretation:

$$2\,A'_3 = \frac{\partial^2 h}{\partial y'^2} = \frac{\partial V_g}{\partial y'},$$ The geostrophic wind shear, positive for cyclonic shear.

$$2\,A'_1 = \frac{\partial^2 h}{\partial x'^2} = V_g\,K_\tau,$$ The geostrophic wind speed x curvature of contours, positive for cyclonic curvature.

$$A'_2 = \frac{\partial^2 h}{\partial x'\,\partial y'} = V_g\,K_n,$$ The geostrophic wind speed x curvature of orthogonals, positive for diverging contours.

4. A comparison of the magnitudes of synoptic geostrophic winds and the observed wind.

Computations were made for seven nets of ten observing stations centered on the radiosonde wind observations at Flint, Dayton, Columbia, Topeka, Amarillo,

Shreveport and Montgomery, for all available observations in the winter season December 1958 through February 1959. This made a total of 1200 comparisons of geostrophic wind and with accompanying wind observation at the 500 mb level and 1123 comparisons at the 300 mb level (of a possible 1274 data periods). The statistics for the observed wind were found to be reasonably consistent with published values based on longer periods of record so the data is believed to provide a representative sample for the winter season. While some variation in the statistics was observed for different stations, it will probably be necessary to examine data for several seasons to establish their significance and for greater generality only average[2] statistics for the five stations with best records are presented in Table I.

Table I Averaged Means and Variance of the Components of the Geostrophic Wind and the Observed Wind.

	500 mb		300 mb	
		Geostrophic Winds		
	mean m sec^{-1}	variance σ^2, m^2 sec^{-2}	mean m sec^{-1}	variance σ^2, m^2 sec^{-2}
V_{gx} (Zonal)	24.12	93.2	36.32	201.6
V_{gy} (Meridional)	-3.86	126.5	-4.48	261.8
		Radiosonde Winds		
V_x (Zonal)	22.84	112.8	34.73	275.7
V_y (Meridional)	-3.10	159.7	-2.70	342.7

2. This average represents the average of the seasonal values for five stations. Shreveport and Montgomery wind records were less regular than the other stations and these data were therefore omitted from the average. The 500 mb average is based on 878 observations while at 300 mb there are 829 observations so that these values should be fairly representative of the winter season in mid-U. S. locations.

The mean observed wind is very nearly equal to the mean geostrophic wind. Since the difference of the means for the individual station were all of similar algebraic sign, the departure of the mean wind from the mean geostrophic wind is believed significant and representative for mid-U.S. The 500 mb mean wind is about 1 m sec^{-1} sub-geostrophic but aligned with the contours, the 300 mb wind is also slightly sub-geostrophic and directed across the contours toward lower heights with a component of the order of 1 m sec^{-1}.

The comparison of observed wind variance and geostrophic wind variance is more significant. The actual wind variance of each component is larger than the geostrophic wind component by about 25% at 500 mb while there is an even greater relative increase at 300 mb. It will be the purpose of the remainder of the analysis to allocate this greater variance of the radiosonde wind among three categories: (1) Synoptic scale accelerations, (2) motions of smaller scale and (3) error in wind measurement.

5. The model for synoptic scale wind variance.

A straightforward method for the analysis of variance according to scale is to compute the autocorrelation function and its Fourier transform. The spatial autocorrelation function of even a two dimensional vector is a tensor that requires four times as much information for its specification as for a scalar autocorrelation. The autocorrelation function for the i and j velocity components, for example, would be:

$$\rho_{ij}(\vec{r}) = \overline{v_i v_j'} \; \sigma_{v_i}^{-1} \; \sigma_{v_j'}^{-1} \text{ where } v_i \text{ and } v_j'$$

are velocity components measured at the ends of the position vector r. It is unlikely that the present radiosonde network can provide satisfactory statistics on a function of this generality. Certainly the 2300 observations used in this

study would not begin to specify this function so that a direct spectral analysis of the wind data did not appear possible. Instead, the statistics for the field of pressure gradient force were found to fit a model of a Gaussian distribution of isobaric height proposed by Buell (1960). This model then provides a filter for the separation of synoptic scale motions from motions of lesser scale. The essentials of Buell's model for the synoptic scale variance of isobaric will therefore be reviewed here.

The distribution of variance of isobaric height is reasonably isotropic as shown by nearly circular isopleths of the autocorrelation coefficients at a number of locations at middle latitudes (Buell, 1958; Bertoni and Lund, 1963). Buell suggested that the isopleths were quite well approximated by the Gaussian distribution function

$$\rho_h (r) = \exp (-r^2/2L^2) \qquad (3)$$

where ρ_h is the autocorrelation function of isobaric height and L is a horizontal scale parameter which is of the order of 1000 km for the mid-troposphere and at middle latitudes. This function not only provides a fairly good description of the autocorrelation isopleths at moderate distances, $r \sim L$, but it also possesses a number of properties that make it suitable for a synoptic scale autocorrelation function. A synoptic scale autocorrelation function of isobaric height must have a second derivative (finite curvature) at the origin, a requirement imposed by the necessity that the geostrophic wind variance must exist for synoptic flow. The curvature of the Gaussian function at the origin is determined by the parameter L and to the extent that the wind is geostrophic the ratio of the variance of observed wind to the variance of isobaric height determines the value of L. The scale parameter L determined from the ratio of wind variance to isobaric height variance is approximately the same as that obtained by fitting the autocorrelation function at greater radius (compare,

for example, values of L deduced by Thompson, 1957, and Buell, 1958).

Buell further deduced if the variance of isobaric height is isotropic and homogeneous the autocorrelation tensor $\rho_{g,ij}$ for synoptic geostrophic[3] winds must be capable of specification by, at most, two correlation functions, the correlation of longitudinal components and the correlation of the transverse components. As in turbulence theory, we shall use the symbols f_g and g_g for the longitudinal and transverse correlations, the subscript g indicating the correlations refer to the geostrophic wind.

The condition that the divergence of the geostrophic wind must vanish leads to the following expressions for the correlation functions. The longitudinal correlation function will have the same form as the autocorrelation function for isobaric height,

$$f_g = \exp(-r^2/2L^2) \tag{4}$$

and the correlation of the transverse components will be

$$g_g = (1-r^2/L^2)\exp\left(-\frac{r^2}{2L^2}\right) \tag{5}$$

Inspection of the trace components of the velocity correaltion tensor for both the geostrophic and actual winds, $\rho_{11}(r)$ and $\rho_{22}(r)$ showed that they did have a shape consistent with the functions (4) and (5) and would be approximated by the same function but with a coefficient less than one. The longitudinal correlation, for example, would be better fit by the function

$$f_g = K_g \exp(-r^2/2L^2), \text{ where } K_g < 1. \tag{6}$$

Of course a real autocorrelation function will approach the value one at the origin. Since the closest spacing between observations is 250 km, an autocorrelation of the form (6) simply indicates a loss in correlation (1-K) in the first computation interval. Put in terms of the spectral distribution of

3. The geostrophic wind is really by definition a quantity defined at synoptic scale so that the adjective synoptic is superfluous used with geostrophic wind as a description of the horizontal pressure gradient force.

variance, it would be interpreted to mean that a fraction of the variance K must be associated with motions of synoptic scale while the fraction (1-K) must be either produced by error or is variance associated with lesser scales. The dimensions of these systems of smaller scale are not precisely determined except that they must be less than twice the spacing of the distance between observing stations. Our hypothetical autocorrelation function would therefore assume a gap in the spectrum of variance between synoptic and lesser scales.

The model autocorrelation function adopted to represent the autocorrelation of both geostrophic and actual winds was of the form suggested by (6). The coefficient K_g was assumed to be the same for both longitudinal and transverse correlations so that where (6) is the expression for the autocorrelation function for the longitudinal components, the autocorrelation function for the transverse velocity components of the geostrophic wind would be given by

$$g_g = K_g \, (1-r^2/L^2) \exp(-r^2/2L^2) \qquad (7)$$

The observed wind autocorrelations were fit by the same type of function but with different coefficients. For the autocorrelation function for the longitudinal components of the observed wind the expression $f_v = K_v \exp(-r^2/2L^2)$ was used, where the subscript v indicates the quantity applied to the observed wind.

Trace components of the correlation tensor were computed for seven pairs of stations for both the 500 mb and 300 mb data for both geostrophic and for actual winds. A single scale parameter L and four values of the parameter K were determined from the 56 data points by a least square fit of the Gaussian functions (6) and (7). Four values of K arise because it was assumed that each level might have a characteristic value of K_g and K_v associated with the geostrophic and actual wind. The quality of the analytic expressions of the type (6) and (7)

as approximations to the autocorrelation fucntion is illustrated by a comparison of the average function for the two orthogonal components with the computed correlations, also averages of two components.

$$1/2\ (f + g) = K(1 - \frac{r^2}{2L^2})\ \exp\ (-r^2/2L^2) \qquad (8)$$

It is possible then to compare each set of observations with a single curve for the function assumed for the autocorrelation function. It must be confessed too that averaging tends to suppress irregularities in the component correlations representing true anisotropics in the wind systems. In Figures 1 and 2 the best fitting average correlation function given by (8) is shown with the average correlation of the trace component of the correlation tensor. If the distribution of isobaric height were truly isotropic, then $1/2\ (\rho_{g\ 11} + \rho_{g\ 22})$ would be equal to the average of the correlations of the longitudinal and transverse components, $1/2(f_g + g_g)$. The individual geostrophic wind correlation points lie above the correlation of the actual wind in every case. The relative magnitude of the intercept K_v and K_g obtained by the least square fit of (8) are clearly established even though there is considerable scatter about the analytic curve. In each correlation set the actual wind correlation is about ten percent less than the geostrophic wind.

6. The variance of the synoptic wind and the geostrophic wind.

The scale parameter L related to the horizontal dimension that was obtained from the fit shown in Figures 1 and 2 was, L = 1071 km, a value much the same as those computed by Buell (1958). The parameters K_v and K_g are(as discussed above and also, for example, by Eddy, 1964) interpreted as that fraction of the total variance associated with the modified Gaussian autocorrelation function which has been assumed to represent the variance at synoptic scale. The equivalent spectrum of the Gaussian autocorrelation function is well known and drops off

rapidly in the wavelength region less than 2L. A wavelength parameter of 1000 km implies that synoptic scale systems have dimensions for the most part greater than 2000 km and systems of dimension L have been completely filtered from the synoptic variance by this autocorrelation function.

The values of the parameters K_v and K_g for the 500 and 300 mb data obtained by a least square fit of the functions of the type given by (7) are shown in Table II. The resulting division of variance at synoptic scale and at lesser scales implied by the analysis is also shown. In all cases, the variance in Table II represents the variance of one component obtained by averaging zonal and meridional components.

Table II Estimate of the magnitude of synoptic wind variance and the variance at smaller scale. (synoptic scale dimension parameter, L = 1071 km).

	Fraction of total variance in synoptic scale motion, K		Synoptic scale variance of one component $K\sigma^2$ $m^2 sec^{-2}$		Smaller scale Variance or error $(1-K)\sigma^2$ $m^2 sec^{-2}$	
	500 mb	300 mb	500 mb	300 mb	500 mb	300 mb
Geostrophic wind K_g	0.940	0.932	103.4	215.9	6.6	15.8
Radiosonde winds K_v	0.817	0.821	111.4	254.0	11.3	55.2

The rather close correspondence of the values of K_g and K_v obtained from the 500 mb and the 300 mb data while not really adding validity to their interpretation as the fraction of variance in synoptic scale has been of some comfort to the analyst. The total variance of the observed wind is so much greater than the total variance of the geostrophic wind that despite its smaller fraction of synoptic variance the variance of the observed wind is greater than the variance of the geostrophic wind in both categories of scale.

The geostrophic wind has really been computed at synoptic scale. The estimate of variance at smaller scale or error for the geostrophic wind is almost entirely variance produced by error in the isobaric height. Indeed, the values (Table II) are consistent with the error estimates of the geostrophic wind made by Endlich and Clark (1963). The greater variance of the observed wind at synoptic scale as compared to the geostrophic wind is assumed to be associated with the geostrophic departures at synoptic scale or the synoptic scale accelerations, $\frac{dV}{dt}$ in Eq. (1). The excess variance of one component is 8.0 m^2sec^{-2} at 500 mb and 28 m^2sec^{-2} at 300 mb. The hypothesis that this difference represents the geostrophic departure of the wind at synoptic scale was investigated further by an analysis of the observed geostrophic departures.

6. The synoptic scale departure of the wind from geostrophic equilibrium.

An independent estimate of the synoptic accelerations (the accelerations measured relative to the coordinate system fixed on rotating earth) is obtained by an analysis of the departure of the observed wind from geostrophic balance. Ideally perhaps, the winds would be smoothed on the same scale as the pressure field and synoptic accelerations computed from the difference. In this study the departures of the observed wind from the synoptic geostrophic wind were computed and the departures subsequently analyzed for evidence of a synoptic scale variation.

Despite very little quantitative evidence, it is almost a meteorological axiom that the geostrophic departures are greater in the direction of the contours, the <u>longitudinal</u> direction, than in the direction across or <u>transverse</u> to the contours. Geostrophic departures were, therefore, computed in natural coordinates as well as in zonal and meridional components. The longitudinal geostrophic departure is indicated by the symbol D_τ and computed thus $D_\tau = V \cos \alpha - V_g$, where α is the angle made by the wind vector with the contours, positive toward high pressure. The transverse geostrophic departure is given

by $D_n = V \sin \alpha$ where V is the observed wind speed. The zonal and meridional components are simply $D_x = V_x - V_{gx}$ and $D_y = V_y - V_{gy}$ positive axis toward the east and north, respectively. Average values for the geostrophic departures for the same five stations as Table I (based on more than 800 cases) are given in Table III.

Table III Statistical characteristics of the departure of the rawinsonde wind from the synoptic geostrophic wind.

	500 mb		300 mb	
	Mean $m\ sec^{-1}$	Variance $\sigma^2 m^2 sec^{-2}$	Mean $m\ sec^{-1}$	Variance $\sigma^2 m^2 sec^{-2}$
Longitudinal Component, D	0.97	31.8	1.16	91.0
Transverse Component, D_n	-0.02	18.4	-1.06	50.9
Zonal Component, D_x	1.28	31.0	1.70	85.4
Meridional Component, D_y	-0.75	18.3	-2.44	50.0

The magnitude of the seasonal mean geostrophic departures of the order of a meter sec^{-1} was already implied when the mean geostrophic wind and mean rawinsonde wind were entered in Table I. The variance of the longitudinal geostrophic departure is significantly larger than the variance of the transverse component. The magnitude of these computed geostrophic departures are perhaps best put in perspective by the diagram in Figure 3. The mean geostrophic wind vector is shown for the 500 mb and the 300 mb levels and the ellipse representing one standard deviation of the departures of the wind from the geostrophic wind is drawn about the terminus of the mean geostrophic wind vector. Typical cross contour angles of the wind (α) are indicated by the vector drawn to the boundary of the ellipse. Thus even though the standard deviation of the zonal component of the wind is almost 20 knots at 300 mb, the typical cross contour angle of 10° is within synoptic experience since the winds

are only reported to the nearest 10° in direction[4].

Since one would like to attach physical significance to the observation that the variance of the longitudinal geostrophic departure is 50% to 75% larger than the variance of the transverse component, it would aid this interpretation if the variance in the zonal and meridional direction were more nearly equal. The zonal departure, however, is the same magnitude as that of the longitudinal component and the meridional component is the same magnitude as the transverse component. Apparently because the wind is so nearly zonal, it is impossible with these data to resolve the precise orientation of the ellipse shown in Figure 3. One is not able to distinguish between the possibility that the observed difference is primarily a zonal-meridional difference or whether it is better related to the direction of the synoptic flow.

To investigate whether, in fact, the geostrophic departures possessed any component at synoptic scale the autocorrelation of geostrophic departures were computed for the same seven pairs of stations. The average correlation of the two components of geostrophic departure are shown as a function of separation in Figure 4. The 300 mb data is sufficiently regular so that a curve of the form of (5) can readily be fitted to the data. The curve shown has the intercept $K = 0.52$, and a horizontal dimension parameter $L = 960$ km, very similar to that found for the geostrophic wind.

The 500 mb geostrophic departure correlations are more irregular and do not clearly exhibit the same horizontal scale as the 300 mb departures. It may be appropriate to consider the extrapolated intercept an upper estimate of the fraction of geostrophic departures at synoptic scale. The estimates of

4. In the climatological data used in this study the wind directions were reported to 1°. It may be of some interest that two large geostrophic departures were ultimately traced to errors remaining in the checked climatological wind data.

synoptic geostrophic departures obtained from the intercept and the variance of the geostrophic departures ($K\,\sigma^2_D$) for one component are as follows:

At 300 mb	36. $m^2 sec^{-2}$
At 500 mb	9.5 $m^2 sec^{-2}$

These are values slightly larger but consistent with the estimate obtained from the excess synoptic variance of the rawinsonde winds. Geostrophic departures are larger at 300 mb than at 500 mb and a larger fraction of the variance of the geostrophic departure has the dimension of synoptic scale. Stating the result in a slightly different way, the synoptic scale wind at 500 mb is more nearly geostrophic and has as a consequence less divergence than the wind at 300 mb.

7. Patterns of synoptic accelerations.

The observation that even with highly curved streamlines and rapidly changing pressure patterns the wind vector remains aligned with the contours has led to many proposals for direct relations between the accelerations and the pressure field or what is equivalent, proposals for mechanisms of adjustment of the wind to geostrophic balance. The equations of motion, on the other hand, predict that accelerations must depend on the initial conditions and a pattern of accelerations related to the pattern of pressure gradient force may be equivalent to requiring a synoptic frictional force of essentially the same magnitude as the synoptic accelerations. The above estimates of the magnitude of synoptic accelerations (that a third to a half ot the observed wind departure from geostrophic may be of synoptic scale) encouraged the test of some features of the models of synoptic acceleration.

Although the derivation of models of acceleration differ (and in some cases do yield conflicting predictions) there is a fundamental uniformity in the prediction that the first approximation to the synoptic acceleration will be

given by the acceleration of the geostrophic wind, $d\vec{V}/dt = d\vec{V}g/dt$ (e.g. Charney, 1955; Bykov, 1962; Petterssen, 1956; Arnasom et al, 1962). The gradient wind approximation can also be construed to be of this form. The only terms of $\frac{dV_g}{dt}$ that can be evaluated on an isobaric chart is the advective component $\vec{V} \cdot \nabla_p \vec{V}_g$ and these terms were computed and compared with the observed geostrophic departures. The geostrophic departures D_τ and D_n were correlated with the components of the geostrophic wind acceleration $[(V \cos \alpha)\ (V_g K_t)]$ and $\{(V \cos \alpha)\ (V_g K_n)\}$ and the results given in Table IV. The relation $\frac{dV}{dt} = \frac{dV_g}{dt}$ implies, among other things, that the wind should be sub-geostrophic with cyclonically curved contours and be directed toward high pressure with converging contours.

Table IV The correlation of the departure of the wind from geostrophic with acceleration of the geostrophic wind.

	500 mb	300 mb
D_τ vs. $[(V \cos \alpha)\ (V_g K_\tau)]$	0.061	0.316
D_n vs. $[(V \cos \alpha)\ (V_g K_n)]$	0.188	0.420
D_τ vs. $[(V \cos \alpha)\ (V_g K_n)]$	0.071	-0.006
D_n vs. $[(V \cos \alpha)\ (V_g K_\tau)]$	0.076	0.052

The first two correlations are those anticipated by the relation $\frac{dV}{dt} = \frac{dV_g}{dt}$; the second set were computed simply as a measure of the noise level in these data.

Neither of the correlations with geostrophic departure with the terms of $\frac{dV_g}{dt}$ are very significant at the 500 mb level but at 300 mb both relations are almost as high as could be expected in view of the previous estimates of small

scale variability of the geostrophic departures. Despite the fact that D_τ is larger than D_n, the correlation of D_τ with the contour curvature term is consistently less than the correlation of D_n with the term involving the convergence of the contours. The slight difference in the correlations does not properly demonstrate the rather marked difference in the quality of the two relations. The two sets of data for 300 mb for Dayton are plotted on scatter diagrams to illustrate this point. In Figure 5, the transverse geostrophic departures are plotted against the geostrophic wind acceleration associated with contour convergence. The line of best fit very nearly corresponds to a line $\frac{dV}{dt} = \frac{dV_g}{dt}$. In Figure 6, which is a scatter diagram for the relation of the longitudinal geostrophic departure plotted versus the geostrophic wind acceleration associated with contour curvature, it is clear the relatively high correlation has not been achieved by a normal distribution about the line $\frac{dV}{dt} = \frac{dV_g}{dt}$.

8. The magnitude of the synoptic friction term.

That the synoptic accelerations can be approximated by the acceleration of the geostrophic wind $\frac{d\vec{V}}{dt} \sim \frac{d\vec{V}_g}{dt}$ has been used to justify the basic assumption employed in the balanced wind, $\frac{d}{dt}(\nabla_p \cdot \vec{V}) = 0$. The balanced wind has also been termed a "frictionless" approximation to the flow (Panofsky, 1957). However, it is readily seen that the observation $\frac{d\vec{V}}{dt} \sim \frac{d\vec{V}_g}{dt}$ may with equal validity be interpreted to mean that the frictional force must be the same magnitude as the synoptic accelerations. If in (1) the geostrophic wind relation is substituted for the horizontal pressure gradient force, one obtains

$$\frac{d\vec{V}}{dt} = f\,\vec{k} \times (\vec{V}_g - \vec{V}) + \vec{F}_n .$$

Differentiation of this expression with respect to time yields

$$\frac{d^2\vec{V}}{dt^2} = f\,\vec{k} \times \left(\frac{d\vec{V}_g}{dt} = \frac{d\vec{V}}{dt} \right) + \frac{d\vec{F}_r}{dt} ,$$

which, with the observation that ($\frac{dV}{dt} = \frac{dV_g}{dt}$), is the relation suggesting $\vec{F}_r = \frac{d\vec{V}}{dt}$.

If the vector standard deviation of the synoptic acceleration is used as a measure of the magnitude of the acceleration and the frictional force, the relative magnitude can best be illustrated as a fraction of the average pressure gradient force at that level. At 500 mb this ratio will be $\sigma\ dV/dt\ (g\ \nabla\ p\ h)^{-1} = 0.16$ and at 300 mb, $\sigma\ dV/dt\ (g\ \nabla\ p\ h)^{-1} = 0.22$. It should not be inferred from this that the frictional force is directly proportional to the pressure gradient force for it is clearly asymmetrical in just the same way as the geostrophic departures are asymmetrical. The meridional or transverse frictional force is perhaps 50% greater than the zonal or longitudinal frictional force. For the same seasons discussed earlier, it is not possible to distinguish between the merits of a model of the frictional force proportional to the geostrophic departure (assumed, for example, by Kao, 1963) or one with a zonal meridional asymmetry as assumed by Davies and Oakes, 1962, either form would be consistent with these data.

The scatter diagram of Figure 6 is cited as evidence for a transverse frictional force of the order of 20% of the mean pressure gradient force at 300 mb. Although the correlation between D_τ and dV_g/dt is significant, the data points spread out in a V-shaped region so that the line dV_g/dt is only a rough bound to the sub-geostrophic departures but large super-geostrophic winds are also found with cyclonically curved contours. Since the transverse geostrophic departures are small and independent of the longitudinal geostrophic departure, it seems clear that the alignment of the wind with the contours can only be maintained by invoking forces other than the synoptic pressure gradient force.

9. The poleward transport of angular momentum.

It is well known that the sink of angular momentum at the surface of the earth in mid-latitudes must be fed aloft by a transfer of momentum from lower latitudes. The transport of angular momentum computed from the correlation of the zonal and meridional wind components is quite variable and dependent upon station location but at mid-continental locations in the central states, it would be expected to be positive at both 500 and 300 mb levels. The correlation of the observed wind components was in fact positive at all stations and the winter five station average correlation coefficient $\overline{v_x v_y} \; \sigma v_x^{-1} \sigma v_y^{-1}$, was computed to be 0.081 at 500 mb and 0.307 at 300 mb. These figures are not necessarily representative of the transport angular momentum at these latitudes but are believed representative of this region for the winter season under investigation. The correlation coefficient for the geostrophic wind components was also computed and while the absolute magnitude of the transport may be in doubt, it was found that the northward transport of angular momentum by the observed wind exceeded the northward transport by the geostrophic wind at all stations and at all levels. The corresponding five station average correlation coefficients for the geostrophic wind were -0.031 and 0.104. It may be concluded therefore that for this region, the poleward transport of momentum occurred largely in the ageostrophic component of the wind.

The transport of angular momentum was investigated further at the 300 mb level where the difference between the correlation coefficients appeared to be most significant. Simply by dividing the cases into either northerly or southerly flow, it was found that on the average north winds were almost parallel to the contours and slightly sub-geostrophic but most of the

difference in the correlation was produced by only 20% of the cases of southerly flow. In southerly flow there is an average geostrophic departure at all stations; the wind speed is super-geostrophic by several meters per second and directed across the contours toward lower isobaric height at an angle of almost 10°. Since southerly flow at 300 mb is usually associated with upward motion and positive wind shear these observed geostrophic departures are consistent with the relation $\frac{dV}{dt} = \frac{dV_g}{dt}$, the geostrophic acceleration in this case being the vertical advection of the geostrophic wind.

In summary, the northward transport of angular momentum at 300 mb is largely produced by geostrophic winds in southerly flow. The wind is on the average slightly super-geostrophic and directed toward lower isobaric height.

10. Summary of results.

The magnitudes of the velocity fluctuations and accelerations determined in this study are summarized by the estimate of the standard deviation of the velocity. Standard deviations of various quantities are given in equivalent velocity fluctuations with units of meters sec^{-1} in Table V. The mean wind speed at each level is tabulated for reference. In view of the sample size the figures have been rounded to the nearest whole number.

Table V Estimated standard deviation of the velocity in meters sec^{-1}, mid-U. S., winter season.

	500 mb	300 mb
Mean Wind Speed	35.0	34.8
Standard deviation		
Observed geostrophic departures all scales		
D_τ longitudinal component	6.	10.
D_n transverse component	4	7
Synoptic scale acceleration of one component, equivalent velocity fluctuation.	3	6
Small scale velocity fluctuation of radiosonde wind (includes error)	3	7
Error of geostrophic wind	2	4

The small scale fluctuation of velocity and the synoptic acceleration are about the same order. The synoptic scale divergence will therefore also be about half the observed divergence a result consistent with a study by Eddy (1964). The synoptic scale vector acceleration is almost 20% as large as the horizontal pressure gradient force. This figure of 20% must also represent an upper magnitude for the frictional force in the free atmosphere.

Appendix: Some characteristics of the synoptic pressure field.

Our ability to filter synoptic scale systems from the background of smaller scale effects and error is largely dependent on the fit of a single parameter Gaussian function to the autocorrelation function for isobaric height. The curves of Figures 1 and 2 illustrate the fit of this function at large distance from the origin and show that the scale parameter L = 1071 km is a correct order of magnitude fit at both the 300 mb and 500 mb levels. Buell (1954) noted that if the horizontal gradient of the variance of isobaric height is small (a condition required for homogeneity) then the curvature of the correlation

function of isobaric height at the origin will be given by the ratio of the variance of the geostrophic wind to the variance of isobaric height. In the notation of the text

$$\frac{\partial^2 \rho_h(0)}{\partial x^2} + \frac{\partial^2 \rho_h(0)}{\partial y^2} = -(f/g)^2 \left[\frac{\sigma^2 v_{gx} + \sigma^2 v_{gy}}{\sigma_h^2} \right] \qquad (1a)$$

If $\rho(r) = \exp\left(- \frac{r^2}{2L^2} \right)$, then the curvature at the origin determines the scale parameter L,

$$L = 2^{1/2} g/f \ \sigma_h \left(\sigma v_{gx}^2 + \sigma v_{gy}^2\right)^{-1/2} \qquad (2a)$$

Values of L obtained from the relation (2a) are consistent with the value of 1071 km obtained in the least square fit of data at large distances from the origin.

Some anisotropies in the field of isobaric height were noted, however, as systematic differences in the magnitude of the second derivatives. At 300 mb in particular the anisotropy could be related to the position of the jet stream and some of the variation in the statistics with station are therefore considered significant. Statistics on the second derivatives of isobaric height at the five stations with most complete records are given in Table (IA). The mean value of the second derivatives for the winter season are tabulated with the standard deviation in units of equivalent vorticity or shear.

Table IA Magnitude of the second derivatives of isobaric height at different stations.
(Units are those of vorticity or shear, seconds^{-1})
Mean and standard derivation for the Winter Season 1958-1959

Station	Geostrophic Shear $g/f\ \partial^2 h/\partial y'^2$		Geostrophic Speed x Contour Curvature $g/f\ \partial^2 h/\partial x'^2$		Geostrophic Speed x Orthogonal Curvature $g/f\ \partial^2 h/\partial x'\ \partial y'$		Geostrophic Vorticity g/f $\frac{\partial^2 h}{\partial x'^2} + \frac{\partial^2 h}{\partial y'^2}$	
	Mean	Std. Deviation	Mean	Std. Deviation	Mean	Std. Deviation	Mean	Std. Deviation
500 mb								
Flint	-0.002×10^{-4}	0.241×10^{-4}	0.109×10^{-4}	0.172×10^{-4}	-0.016×10^{-4}	0.106×10^{-4}	0.107×10^{-4}	0.345×10^{-4}
Dayton	-0.006	0.252	0.138	0.186	-0.048	0.130	0.133	0.379
Topeka	-0.068	0.226	0.051	0.190	-0.036	0.113	-0.016	0.326
Columbia	-0.098	0.235	0.083	0.202	-0.029	0.111	-0.015	0.354
Amarillo	0.002	0.206	0.106	0.197	-0.012	0.099	0.107	0.334
300 mb								
Flint	0.044×10^{-4}	0.328×10^{-4}	0.141×10^{-4}	0.252×10^{-4}	-0.023×10^{-4}	0.148×10^{-4}	0.185×10^{-4}	0.498×10^{-4}
Dayton	0.039	0.344	0.189	0.262	-0.065	0.163	0.228	0.525
Topeka	0.048	0.337	0.081	0.316	-0.048	0.175	0.033	0.522
Columbia	-0.107	0.310	0.076	0.280	-0.037	0.189	-0.031	0.482
Amarillo	-0.006	0.311	0.166	0.324	- .017	0.160	0.160	0.528

The seasonal average of the second derivatives are small at all stations. A small cyclonic curvature and a slight confluence of the mean contours is observed at all stations as indicated by the positive values of the mean derivative $\frac{\partial^2 h}{\partial x'^2}$ and the negative values of the mean derivative $\frac{\partial^2 h}{\partial x \partial y'}$. This pattern of contours also appears in published mean seasonal contour charts at these locations.

The distribution of values of the derivatives measured in natural coordinates closely approaches a normal distribution so that the standard deviation provides a good estimate of the representative magnitudes. For example, in only one case did the anti-cyclonic geostrophic shear exceed the value of the Coriolis parameter, a value approximately three standard deviations from the mean. The principal anisotropy shown by these data is the tendency towards a zonal or longitudinal striation as shown by the consistently greater magnitude of the geostrophic shear as compared to the longitudinal second derivative associated with contour curvature. Only at Amarillo is there approximate isotropy in the second derivatives.

The smaller magnitude of the cross derivative, $\frac{\partial^2 h}{\partial x' \partial y'}$, does not indicate anisotropy. It is instead a measure of the ratio of the amplitude of synoptic scale velocities to the speed of the zonal current. In any case, these derivatives have almost the same magnitude at a given level at all stations.

The vorticity variance is approximately that given by the sum of the variance of each derivative indicating almost no correlation in the component second derivatives. The vorticity increases by at least fifty percent from 500 to the 300 mb level and is remarkably uniform with station location.

The magnitude of the second derivatives can be illustrated in another fashion by a computation of typical values of the contour radius of curvature and radius of curvature of the orthogonals. A radius of curvature of the contours was computed from the ratio of the mean geostrophic wind speed to the standard deviation

of the longitudinal derivative

$$R_c = \overline{V}_g \quad f/g \quad \sigma_{\left(\frac{\partial^2 h}{\partial x'^2}\right)}^{-1}$$

This is in effect another measure of the size of pressure systems; values of the radius of curvature of the contours calculated at these stations is given in Table IIA. The values vary with the station location but are almost constant with altitude.

Values of the orthogonal curvature showing convergence or divergence of the contours are computed in similar fashion from the standard deviation of the cross derivative. The orthogonal curvature is almost constant with altitude. Typical values of orthogonal curvature are given in Table IIIA.

In conclusion the characteristic of the synoptic scale field of isobaric height are fairly well summarized as isotropic disturbances on a zonal current with a horizontal scale greater than 1000 km. The scale of the systems is not greatly different at 500 and 300 mb. The major anisotropy is the longitudinal striation associated with what might be called the jet stream.

Table IIA Typical values of radius of curvature of the contours, km. Another measure of the size of pressure systems.

	500 mb	300 mb
Flint	1540 km	1500 km
Dayton	1600	1680
Columbia	1240	1300
Topeka	1190	1090
Amarillo	950	950

Table IIIA Typical values of the radius of curvature of contour orthogonals, km. A measure of the degree of confluence of the contours.

	500 mb	300 mb
Flint	2500 km	2560 km
Dayton	2290	2710
Columbia	1930	1930
Topeka	1990	1970
Amarillo	2240	1920

FIGURE CAPTIONS

Fig. 1 Average autocorrelation of trace components of the geostrophic wind (solid circles) and rawinsonde wind (open circles) for the 500 mb level. The curve is the least square fit of the function, $K(1-r^2/2L^2)\exp\left(-\frac{r^2}{2L^2}\right)$.

Fig. 2 Average autocorrelation of trace components of the geostrophic wind (solid circles) and rawinsonde wind (open circles) for the 300 mb level. The curve is the least square fit of the function, $K(1-r^2/2L^2)\exp\left(-\frac{r^2}{2L^2}\right)$.

Fig. 3 Illustration of representative total departure of the wind from geostrophic computed in this study. The mean geostrophic wind vector is plotted to scale and ellipses of semi major and semi minor axes of one standard deviation of the zonal and meridional geostrophic departures are drawn about the terminus of each vector. The cross contour angle should lie within the angle α about two thirds of the time.

Fig. 4 Average autocorrelation of orthogonal components of the departure of the wind from geostrophic. Solid circles 300 mb data, open circles 500 mb data. The curve is the fit of the function $K\left(1-\frac{r^2}{2L^2}\right)\exp -\frac{r^2}{2L^2}$ to the 300 mb data.

Fig. 5 Scatter diagram of the relation between the transverse geostrophic departure and the longitudinal component of geostrophic acceleration. Example of Dayton data 300 mb. The broken line represents the relation predicted by the assumption

$$\frac{d\vec{V}}{dt} = \frac{d\vec{V}_g}{dt}$$

Fig. 6 Scatter diagram of the relation between the longitudinal geostrophic departure and transverse component of geostrophic acceleration. Example of Dayton data 300 mb. The broken line represents the relation predicted by the assumption

$$\frac{d\vec{V}}{dt} = \frac{d\vec{V}_g}{dt} .$$

REFERENCES

Arnason, G., G. J. Haltiner and M. J. Frawley, 1962: Higher-Order Geostrophic Wind Approximations., Mon. Wea. Rev. 90, 175-185.

Buell, C. E., 1954: Some Relations Among Atmospheric Statistics., J. Meteor. 11, 238-244.

Buell, C. E., 1957: An Approximate Relation Between the Variability of the Wind and the Variability of Pressure or Height in the Atmosphere. Bull. Amer. Meteor. Soc., 38, 47-51.

Buell, C. E., 1958: The Correlation Between Wind and Height on an Isobaric Surface II: Summer Data. J. Meteor., 15, 502-512.

Buell, C. E., 1960: The Structure of Two Point Wind Correlations in the Atmosphere, J. Geophys. Res., 65,3353-3366.

Bykov, V. V., 1962: On Taking Account of the Geostrophic Departure in Short Range Forecasting, Izv. Geophys. Ser., 3, 418-423, English Edition 277-279.

Charney, J., 1955: The Use of the Primitive Equations of Motion in Numerical Prediction, Tellus, 7, 22-26.

Corby, G. A., 1961: Some Experiments on the Objective Analysis of Contour Charts., Quart. J. R. Meteor. Soc., 87, 34-42.

Davies, D. R. and M. B. Oakes, 1962: On the Problem of Formulating a Realistic Model of the General Atmospheric Circulation, J. Geophys. Res., 67, 3121-3128.

Eddy, A., 1964: The Objective Analysis of Horizontal Wind Divergence Fields, Quart, J. R. Meteor. Soc. 90, 424-440.

Endlich, R. M. and J. R. Clark, 1963: Objective Computation of Some Meteorological Quantities, J. Appl. Meteor., 2, 66-81.

Endlich, R. M. and G. S. McLean, 1965: Jet Stream Structure over Central United States Determined from Aircraft Observations, J. Appl. Meteor., 4, 83-90.

Kao, S. K., 1962: Large-Scale Turbulent Diffusion in a Rotating Fluid with Applications to the Atmosphere, J. Geophys. Res. 67, 2347-2359.

Miller, J. R., 1951: Energy Equations in Compendum of Meteorology, Boston, Amer. Meteor. Soc., 483-491.

Panofsky, H., 1958: Introduction to Dynamic Meteorology. University Park, College of Mineral Industries, the Pennsylvania State University 243 pp.

Petterssen, S., 1956: Weather Analysis and Forecasting, Vol. I, New York, McGraw Hill, 428 pp.

Thompson, P. P., 1957: The Relation of Standard Deviation of Contour Heights and Standard Deviation of the Wind, Quart. J. R. Meteor. Soc. 83, 554-555.

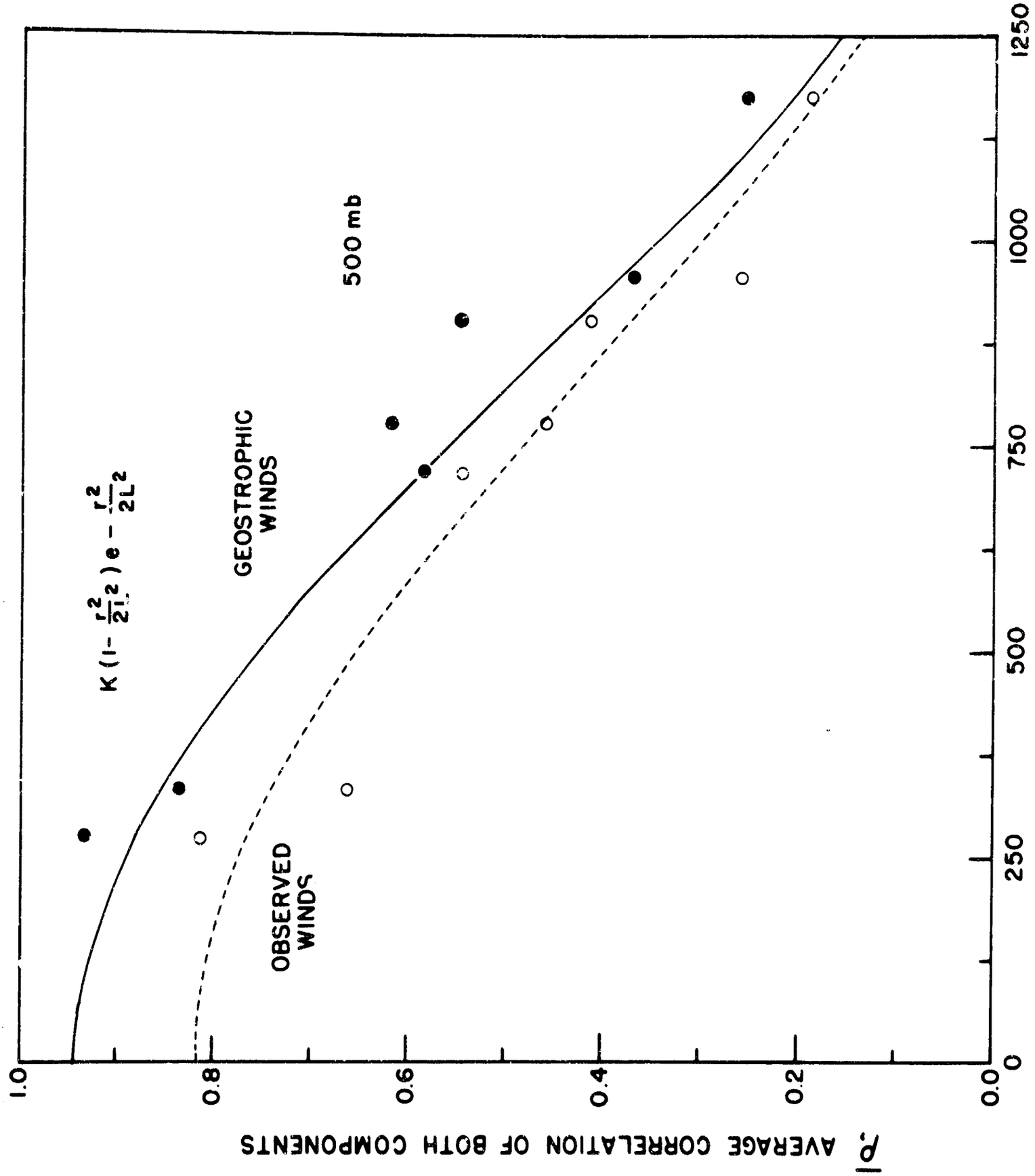
$K\left(1-\frac{r^2}{2L^2}\right)e^{-\frac{r^2}{2L^2}}$
GEOSTROPHIC WINDS
500 mb
OBSERVED WINDS
1.0
0.8
0.6
0.4
0.2
0.0
0
250
500
750
1000
1250
$\overline{\rho}$, AVERAGE CORRELATION OF BOTH COMPONENTS

Fig. 1

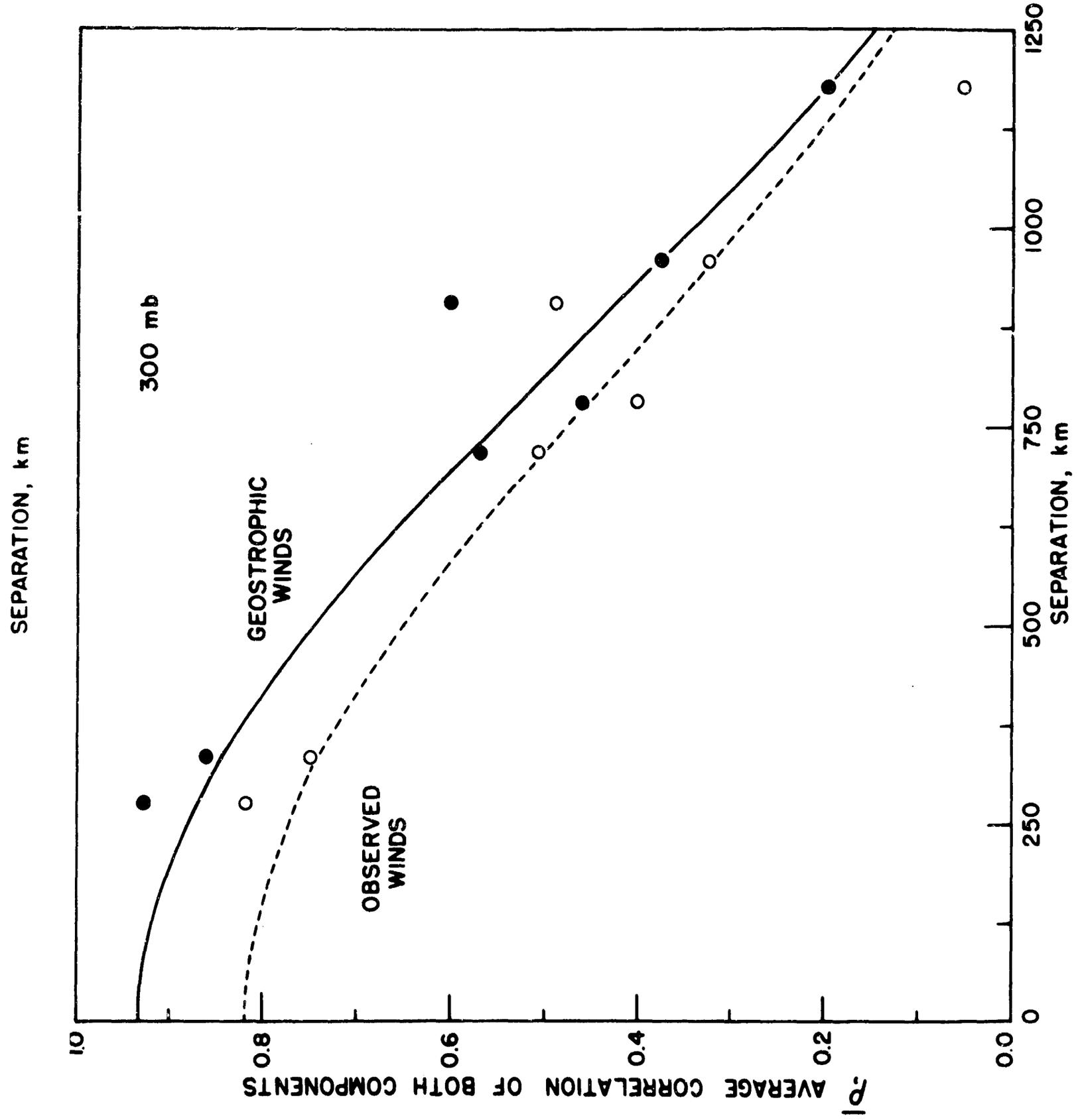
300 mb
GEOSTROPHIC WINDS
OBSERVED WINDS
SEPARATION, km
SEPARATION, km
$\overline{\rho}$ AVERAGE CORRELATION OF BOTH COMPONENTS
1.0
0.8
0.6
0.4
0.2
0.0
0
250
500
750
1000
1250

Fig. 2

SEPARATION, KM

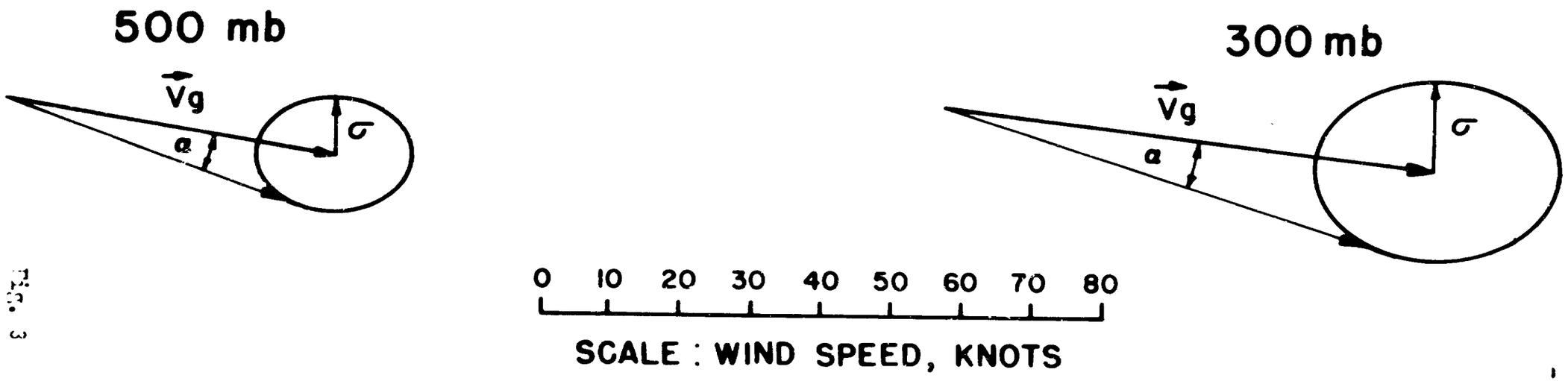

Fig. 3

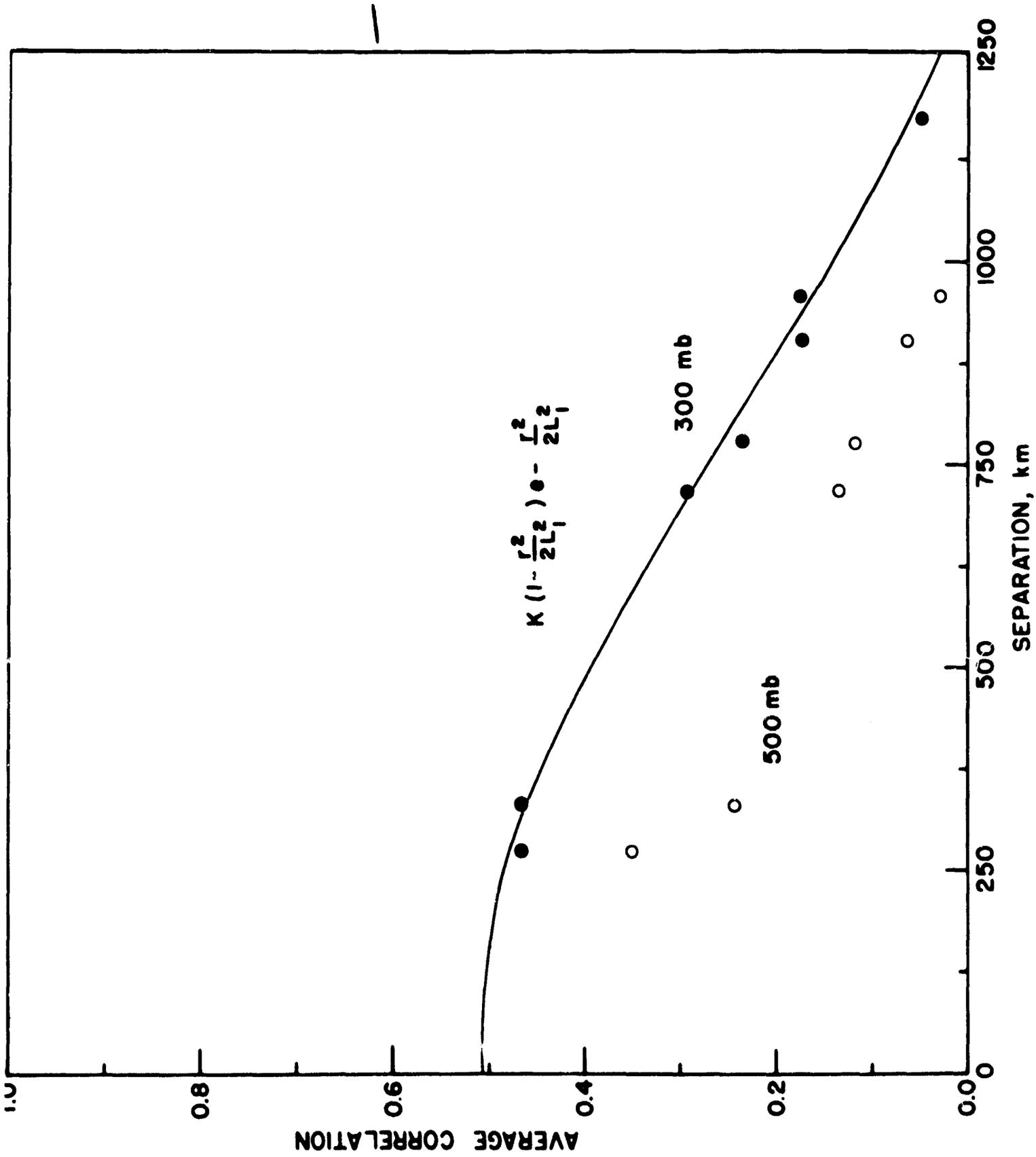
AVERAGE CORRELATION
1.0
0.8
0.6
0.4
0.2
0.0
0
250
500
750
1000
1250
SEPARATION, km
300 mb
500 mb
$K\left(1-\frac{r^2}{2L_1^2}\right)e^{-\frac{r^2}{2L_1^2}}$

Fig. 4

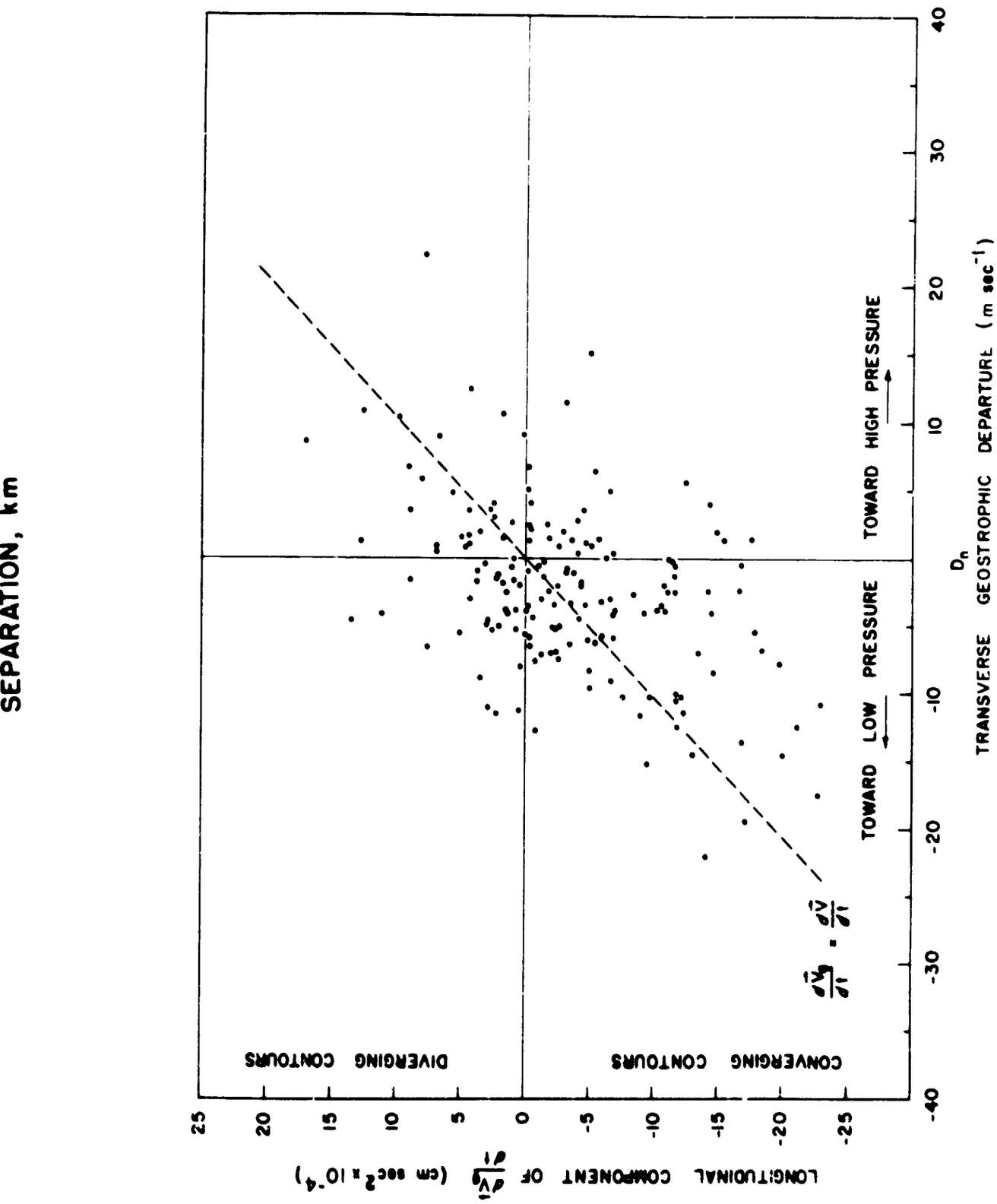
SEPARATION, km
LONGITUDINAL COMPONENT OF $\frac{dV_g}{dt}$ (cm sec^{-2} x 10^{-4})
25
20
15
10
5
0
-5
-10
-15
-20
-25
DIVERGING CONTOURS
CONVERGING CONTOURS
$\frac{dV_g}{dt} = \frac{dV}{dt}$
TOWARD LOW PRESSURE
TOWARD HIGH PRESSURE
-40
-30
-20
-10
10
20
30
40
D_n
TRANSVERSE GEOSTROPHIC DEPARTURE (m sec^{-1})

Fig. 5

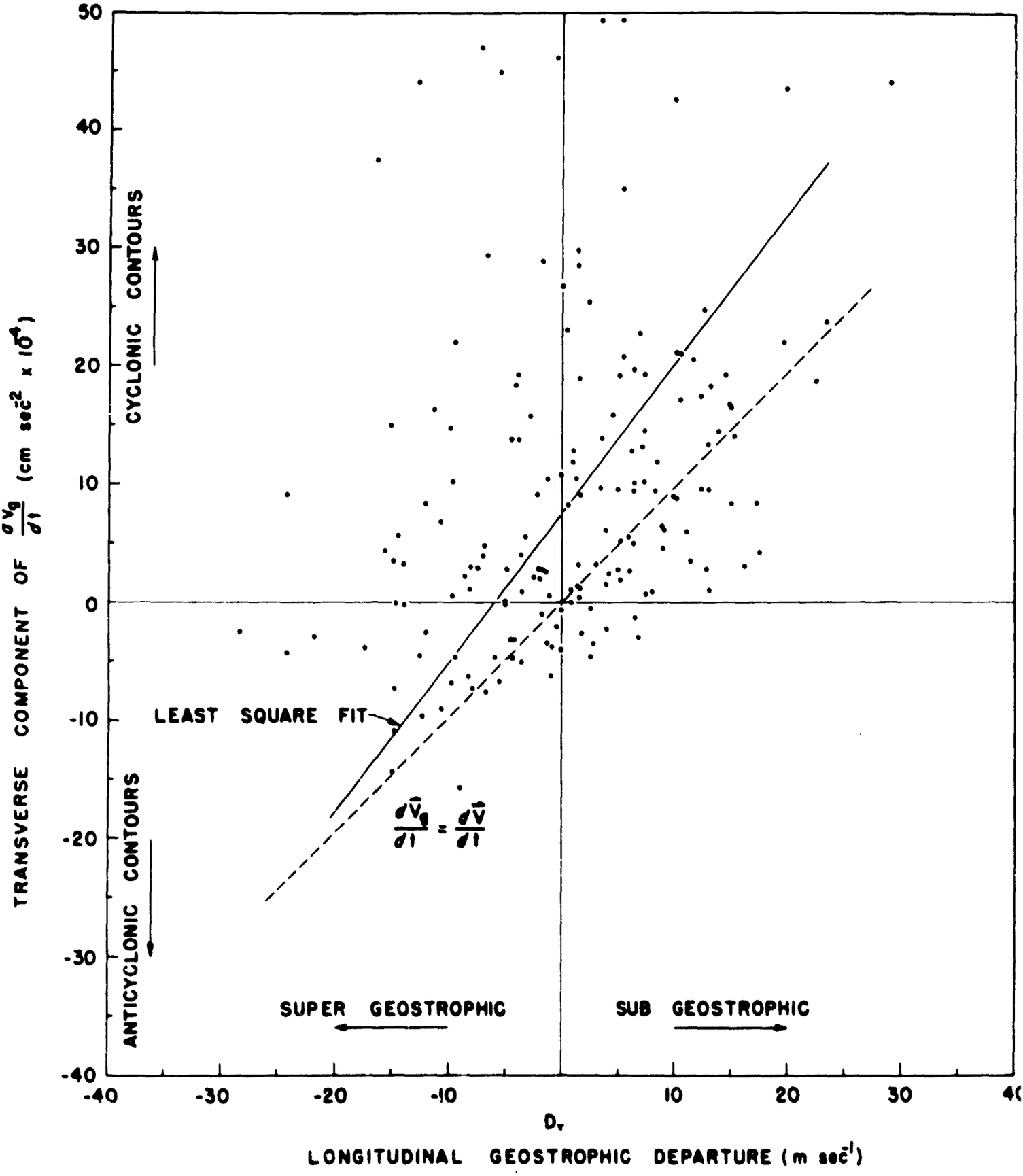
50
40
30
20
10
0
-10
-20
-30
-40
-40
-30
-20
-10
10
20
30
40
CYCLONIC CONTOURS
ANTICYCLONIC CONTOURS
LEAST SQUARE FIT
$\frac{d\vec{V}_g}{dt} = \frac{d\vec{V}}{dt}$
SUPER GEOSTROPHIC
SUB GEOSTROPHIC
TRANSVERSE COMPONENT OF $\frac{dV_g}{dt}$ (cm sec^{-2} x 10^{-4})
D_T
LONGITUDINAL GEOSTROPHIC DEPARTURE (m sec^{-1})

Fig. 6

The Vertical Distribution of Dust

by

James M. Rosen

Six flights have been made with a coincidence type dust counter similar to the one previously described (Ann. Prog. Report, 1964). The results of two of these flights have already been reported, (Rosen, 1965, 1966).

The first flight made with the coincidence dust counter is a good illustration of the layered character of the stratosphere. The data are shown in Figures 1 and 2. The region between the tropopause and the ozone maximum is frequently characterized by dust and ozone rivers described by Kroening and Ney (1962). On this sounding there appears to be a good correspondence between the two lower dust and ozone peaks. At 19.5 km however, there is an ozone river but no corresponding dust river. This observation may seem in conflict with the hypothesis that the dust and ozone are transported together but can be understood by referring to the lines of constant mixing ratio on the sounding. Since the mixing ratio of a trace constituent is preserved in vertical displacements a river will not appear in a sounding for that constituent in a region where the mixing ratio is constant with altitude. The river in this case is in a location where the dust follows a constant mixing ratio with altitude but the ozone does not. Thus, only the ozone profile should show the river. Above the ozone maximum where both the dust and ozone mixing ratio is constant with altitude a river cannot be observed in a sounding for these constituents.

A casual inspection of the dust and ozone layers at about 17 km would suggest that it is also a river, but upon closer examination a number of peculiarities appear normally not associated with rivers. First, the dust layer is about 1 km lower than the ozone layer (the resolution is about 1/6 km).

Second, the mixing ratio of dust in this layer is greater than at any point in the atmosphere above it. In addition, the size distribution in this layer is considerably different from that of the surrounding atmosphere (Figure 2).

This layer is perhaps associated with the radioactive debris from the underground explosion in Nevada two weeks before the flight or from the Chinese explosion six months before the flight,or from high altitude testing two years before the flight. The first two sources seem rather unlikely in view of the fact that there was very little fallout connected with them (Kuroda et al, 1965). The third source also does not seem very likely because there is over two years between injection and measurement. However, thin radioactive layers in the stratosphere were observed over Alaska in February of 1965 (Wong, 1965). Thus, it may be possible that the layer at 17 km is connected with radioactive debris.

The dust distribution above 17 km is characterized in this sounding by layers in which the mixing ratio is constant with altitude but discontinuous at the boundaries. Another peculiar layer appears at 26 km. The size distribution in this layer is extremely different from the surrounding atmosphere. This layer is also marked in the ozone by a change in the profile structure, not by a change in concentration.

A meaningful analysis of the dust and ozone profile can only be made when enough data is available to identify the same phenomenon in more than one flight. A comprehensive review and analysis of the entire data obtained from this projecy is forthcoming.

REFERENCES

1. Kroening, J. L. and E. P. Ney, J. Geophys. Res. 67, 1867-1875 (1962).

2. Kuroda, P. K., B. D. Palmer, M. Attrap, J. N. Beck, R. Granapathy, D. D. Saber and M. N. Rao, Fallout from the N uclear Explosion of 16 October, 1964, Science 147, 1284-1286 (1965).

3. Rosen, J. M. , Dust in the Stratosphere, Conference on Cosmic Dust, Smithsonian Contributions to Astrophysics, Cambridge, (1965) in press.

4. Rosen, J. M., Correlation of Dust and Ozone in the Stratosphere, Nature Vol. 209, No. 5030, p. 1342 (1966).

5. Wong, Y. S., Radioactive Debris over Fairbanks, Alaska, on February 18, 1965, J. Geophys. Res. 71, 1766-1767 (1965).

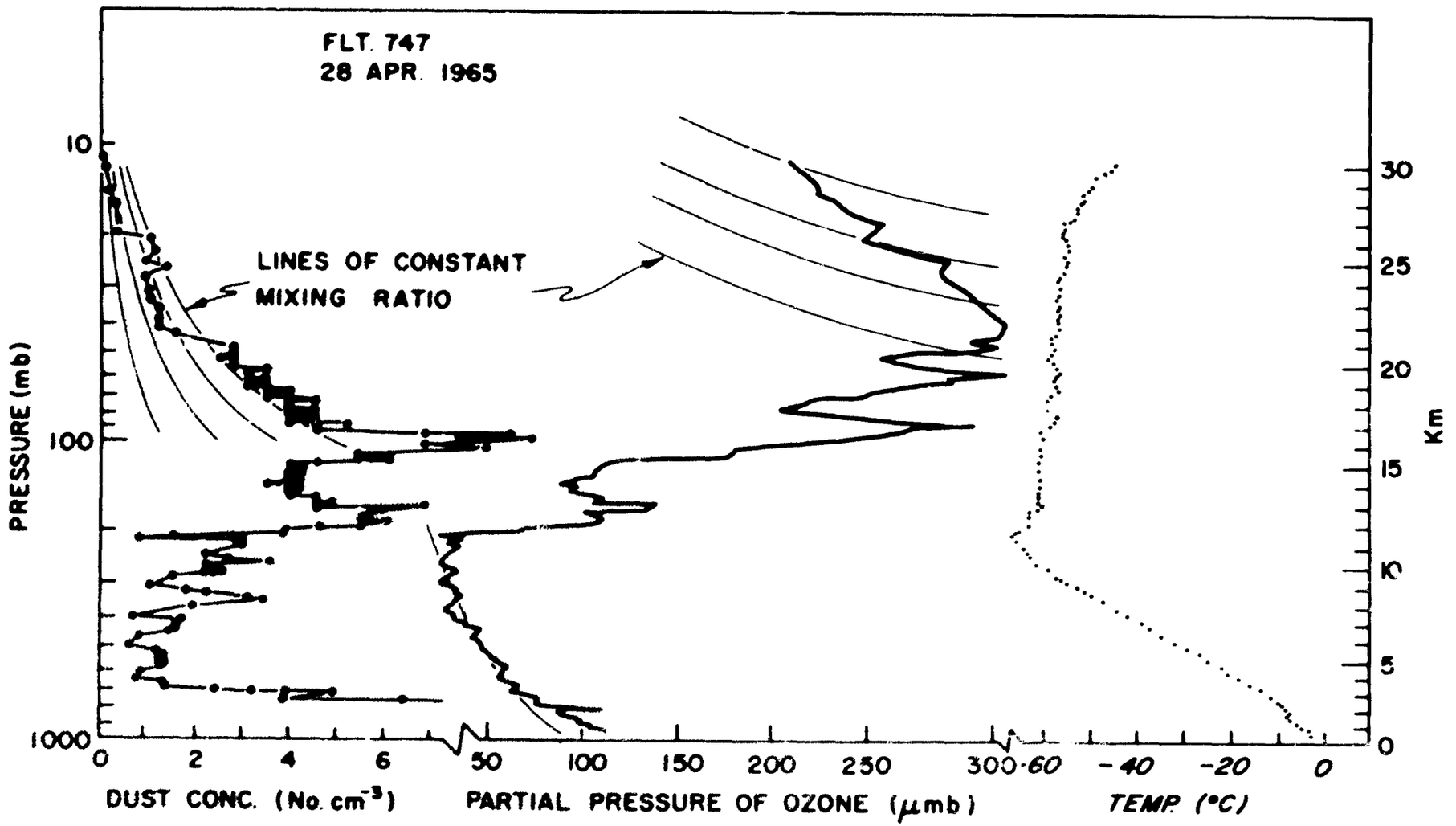

The dust and ozone concentration and temperature profile on ascent of Flt. 747. The dust concentration refers to all particles with .25 microns diameter and larger.

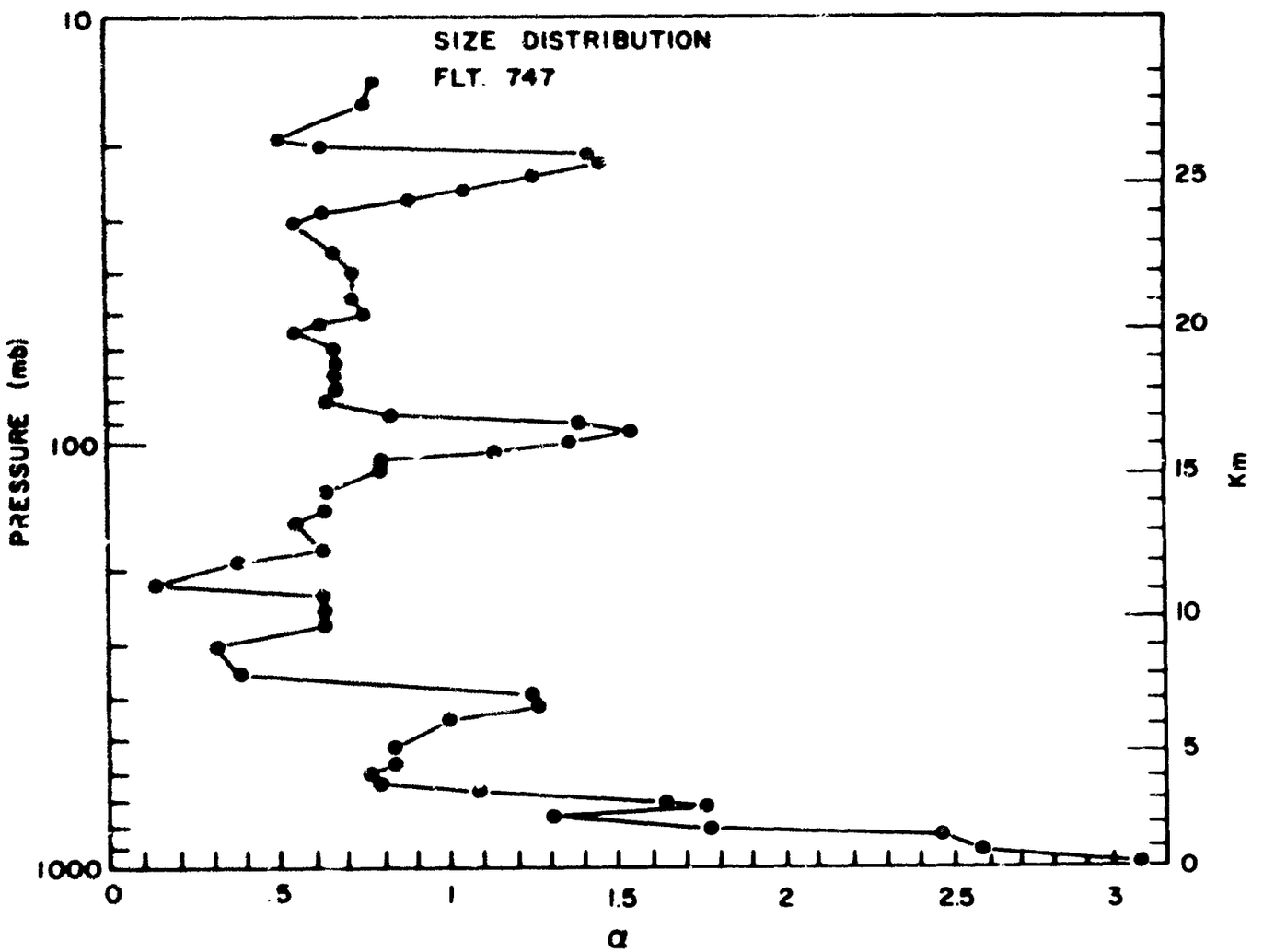

Internal size distribution on ascent of Flt. 747. An internal size distribution of the form $r^{-\alpha}$ has been assumed (radius of dust).

Solar Extinction

by

F. C. Gillett and T. J. Pepin

A number of high altitude balloon flights have been made with an instrument to measure the extinction of sunlight during sunrise as the path length of the ray in the atmosphere varies with the sun's position on the horizon to 8° above the horizontal. These measurements are similar in kind and purpose to the measurements of stellar extinction reported previously (Ann. Prog. Report 1965). Although the phenomenon of "scintillation" cannot be observed a measurement of solar extinction has the basic advantage of increased light level which allows a wide choice of detectors and spectral ranges for investigation.

These first experiments were designed to supplement the direct measurements of dust and ozone and the extinction was measured in three different wave length bands which would best distinguish between the effects of these constituents. Photocells were used as detectors to measure the extinction in a band near 4500 A°, 6000 A° and 8500 A°. The extinction in the 4500 A° region is primarily Rayleigh scattering by air molecules with only a small contribution due to scattering by dust. The band at 6000 A° is at the maximum of the Chappius absorption by ozone and the extinction in this band will be primarily produced by ozone absorption. In the infrared region, the 8500 A° band, the extinction should be produced mostly by dust scattering with only a small amount of Rayleigh scattering. The data on solar elevation and intensity have been reduced to a plot of intensity as a function of air mass and in this form (on a semi-log plot), there is found for all three wave length regions a linear variation at small path lengths. This makes it possible to define an extinction coefficient for the upper atmosphere from the relation: $I=I_0 \exp(-kX)$ where X is the path

length in units of air mass. The extinction coefficient in the infrared (8500 A° band) was found to be highly variable. The maximum value of K_{IR} observed was 0.14 on 28 August 1965 and a minimum of 0.07 on 11 November 1965, a change attributed to an equivalent change in the number density of small dust particles in the upper atmosphere.

Preliminary analysis has also been performed on the data from one of these flights on rays passing through the atmosphere lying below the balloon to determine the vertical distribution of dust down to the tropopause. The results of this analysis obtained by a numerical transformation of the data on extinction as a function of atmospheric path is shown in Figure 1 where the product of the number density of dust particles times effective scattering cross section for the dust is plotted against altitude. That these values of dust concentration are consistent with the direct measurements by Rosen (1966) may be appreciated by assuming a characteristic size of 0.5μ for the scattering particles. The maximum concentration just above the tropopause then corresponds to a number density of several dust particles cm^{-3}.

On the basis of one calculation, this method of analysis looks very promising and will be applied to the data collected in the other flights of this series to determine the product of the dust density and effective scattering cross section as a function of altitude. It can further be extended to the extinction results observed in the ozone absorption band to determine the ozone concentration as a function of altitude and by proper choice of spectral region in the infrared region of the spectrum, perhaps the H_2O content of the atmosphere at high altitudes can be measured.

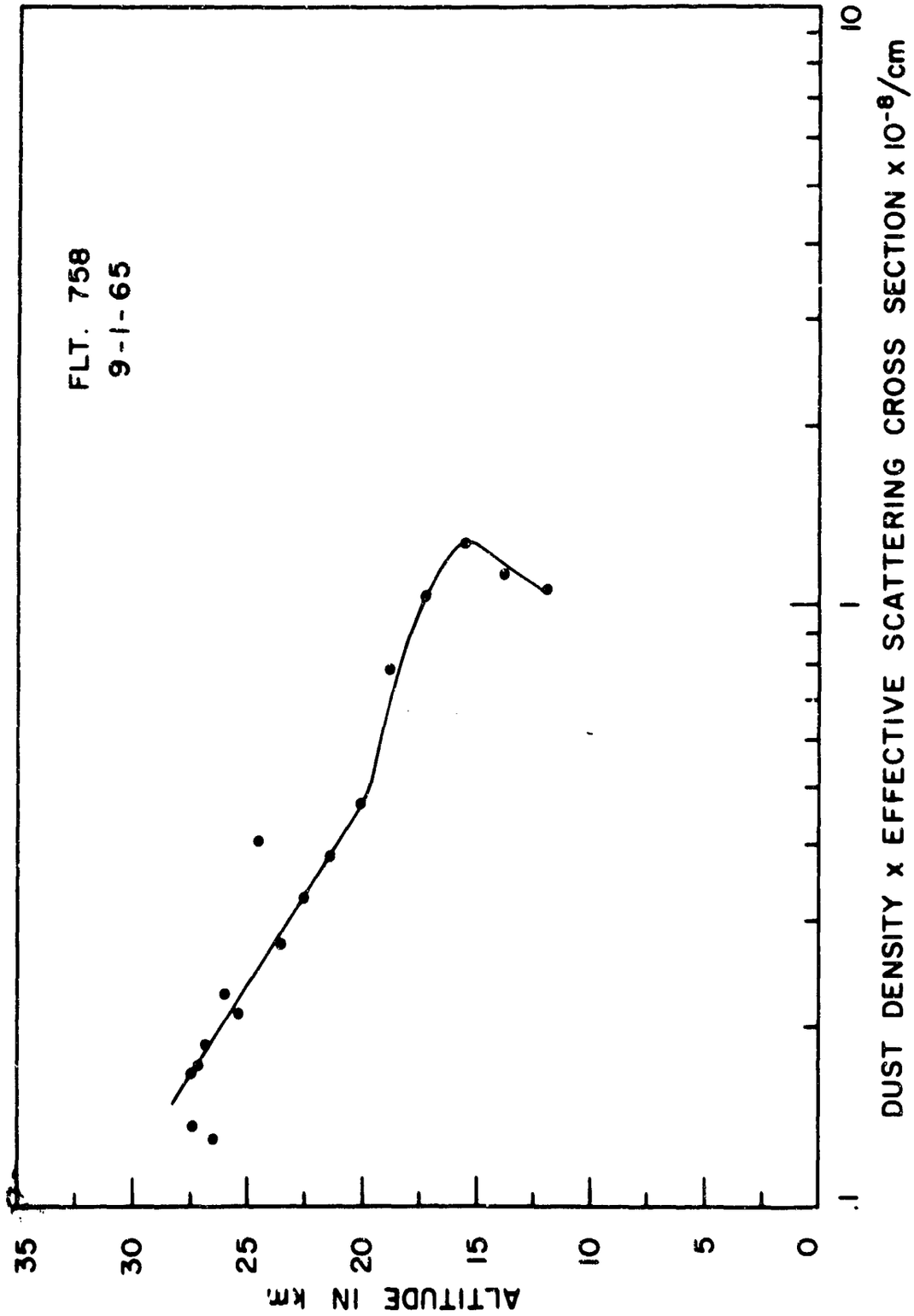
FLT. 758
9-1-65
ALTITUDE IN KM
35
30
25
20
15
10
5
0
.1
1
10
DUST DENSITY x EFFECTIVE SCATTERING CROSS SECTION x 10^-8/cm

Fig. 1

Dust Collection from the Stratosphere

by

James M. Rosen

An effort is being made to collect a small amount of stratospheric dust for study in the laboratory. The instrumentation has already been developed and filter samples will be taken in the near future.

A comparison of the results of this experiment with those of the photoelectric dust counter will show what portion of the particles are opaque and perhaps will indicate how the aerosol concentration in the stratosphere is altered by water vapor. The origin of the dust can be determined by looking for cosmogenic nuclides induced by the solar wind. Chemical analysis however, will not be possible with the small sample obtained.

Figure 1 shows the probable size distribution of dust at 50 mb. This graph can be used to estimate the largest particle that will be collected on the filter. Since the sampling volume is 3×10^5 cm^3, the largest particle expected is about 6 microns diameter. Note that a volume of 100 cubic meters would be necessary to obtain a few particles of 20 micron diameter.

The dust on the filter will be altered in two ways from its natural state in the stratosphere: first, the volatile component (such as water vapor) will have disappeared and second, only the opaque particles will be observable.

It is necessary to have a reasonable number of dust particles per field of view in the microscope to insure a reliable count. The filter area (1 cm^2) has been chosen so that there will be about 20 particles per field of view with diameters greater than .5 microns. Experience has shown that the size distribution can be determined reliably down to .3 microns diameter using standard light microscope techniques. It is not necessary to have as high a surface concentration of large particles because they are easier to observe.

A schematic diagram of the sampling instrument is shown in Figures 2 and 3. The vacuum tank draws air through the filter after the balloon reaches ceiling. The filters are kept covered except during the sampling period. When the filters are covered, the filter chamber is vented to the outside through a breathing filter. Thus, the dead air space behind the sampling filter cannot draw in polluted air during descent. After sampling has been completed, valve #1 is closed and the vacuum tank is opened to the atmosphere through valve #2. This prevents any contamination that might arise from a leak in valve #1. The operation of the valves and filter cover is monitored and transmitted back to a ground receiving station. In addition, air temperature and pressure is measured both inside and outside the tank.

REFERENCES

1. Alexander, W. M., C. W. McCracken, L. Secretan and O. E. Berg, Review of Direct Measurements of Interplanetary Dust from Satellites and Probes., Goddard Space Flight Center, Greenbelt, Maryland.

2. Hamilton, W. L., and C. Buell, A Comparison of Dust Flux in the Upper Atmosphere and on the Polar Ice Sheets. J. Geophys. Res. 71, No. 10, p. 2679 (1966).

3. Hemenway C., Balloon-top Collections from Meteor Showers., The Cambridge Cosmic Dust Conference., Smithsonian Contributions to Astrophysics (1965), to be published.

4. Junge, C. E., C. W. Chagnon, J. E. Manson, Stratospheric Aerosols, J. Meteor. 18, pp. 81-108 (1961).

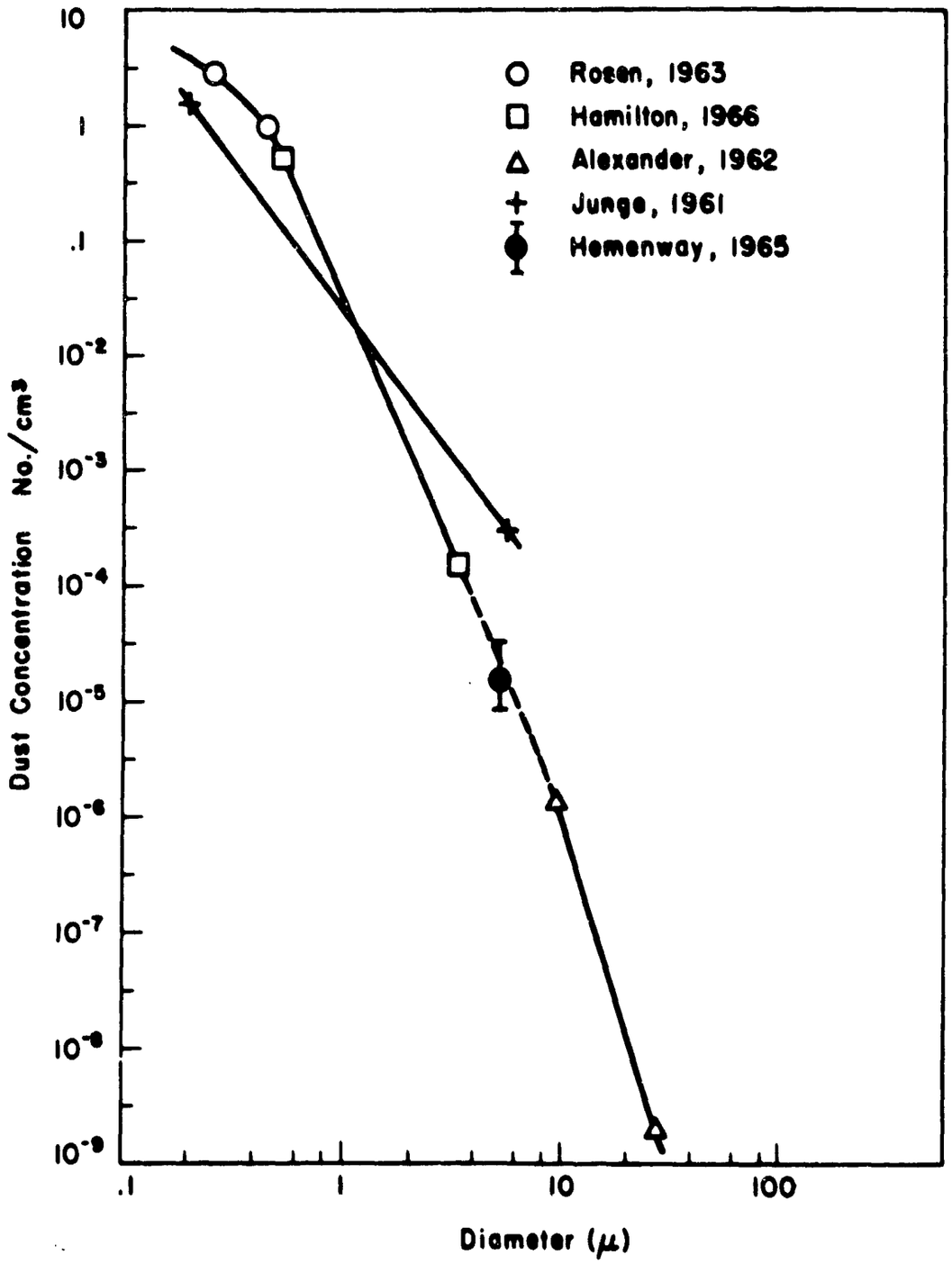

Fig. 1

The integral size distribution of dust particles at 50 mb.

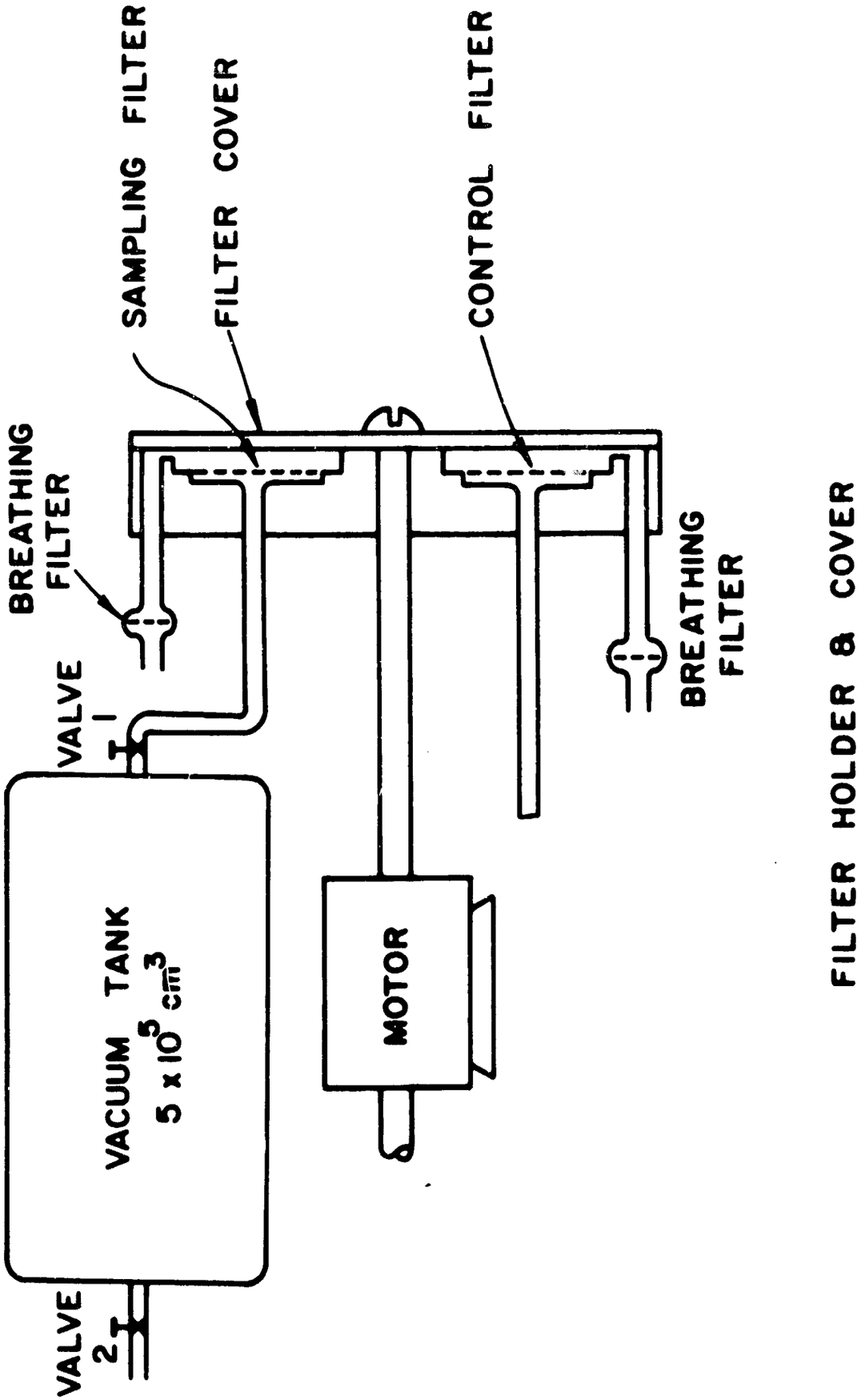

Fig. 2

Schematic diagram of sampling mechanism.

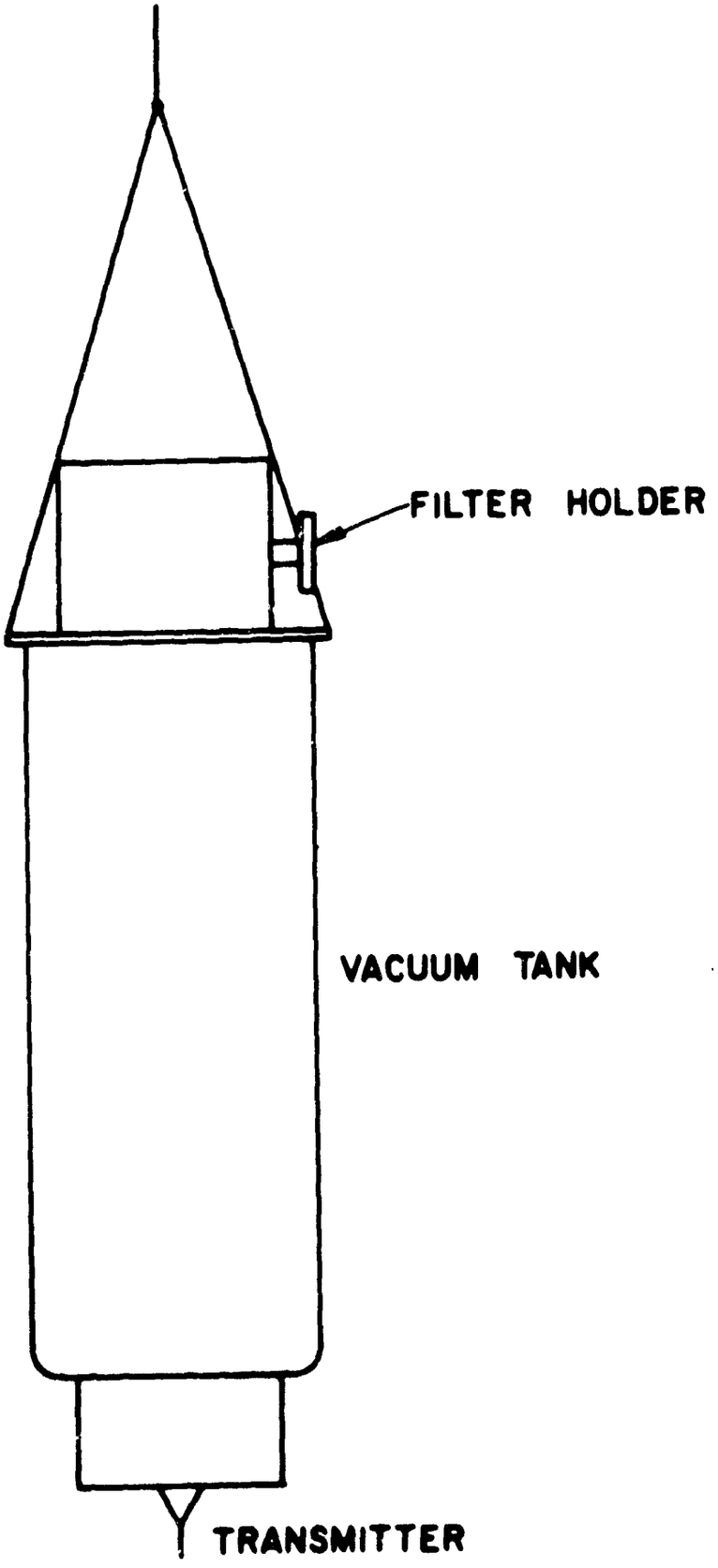

- Fig. 3

The instrument package for stratospheric dust sampling.

Stellar Extinction and Scintillation

Although no further stellar extinction measurements have been made this past year, there has been some development of the observation technique and analysis. Stellar extinction measurements in principle may be used for the same purpose as solar extinction measurements and have the advantage of extending the observing period beyond the few minutes of sunrise or sunset. These measurements might be used to detect, for example, the diurnal variation of a constituent. Because of the much smaller dimension of the stellar beam, it is also possible to observe smaller scale fluctuations in intensity that may be associated with smaller scale inhomogeneities in the atmosphere. It is anticipated, therefore, that some further exploratory measurements of stellar extinction will be made.

Security Classification

DOCUMENT CONTROL DATA - R&D

(Security classification of title, body of abstract and indexing annotation must be entered when the overall report is classified)

1 ORIGINATING ACTIVITY *(Corporate author)*
School of Physics and Astronomy
University of Minnesota
Minneapolis, Minnesota 55455

2a REPORT SECURITY CLASSIFICATION
Unclassified

2b GROUP

3 REPORT TITLE

ANNUAL PROGRESS REPORT

4 DESCRIPTIVE NOTES *(Type of report and inclusive dates)*
Progress Report

5 AUTHOR(S) *(Last name, first name, initial)*
Homer T. Mantis
James M. Rosen
F. C. Gillett and T. J. Pepin

6 REPORT DATE
June 1966

7a TOTAL NO. OF PAGES
51

7b NO. OF REFS
26

8a CONTRACT OR GRANT NO.
Nonr-710(22)

b PROJECT NO

c

d

9a ORIGINATOR'S REPORT NUMBER(S)
AP-24

9b OTHER REPORT NO(S) *(Any other numbers that may be assigned this report)*

10 AVAILABILITY/LIMITATION NOTICES
Distribution of this document is unlimited.

11 SUPPLEMENTARY NOTES

12 SPONSORING MILITARY ACTIVITY
Department of the Navy
Office of Naval Research
Washington, D. C. 20360

13 ABSTRACT

A review of the research performed by the Atmospheric Physics Group of the University of Minnesota for the year ending June, 1966. The work reported is in three distinct areas: (1) Atmospheric Motions, (2) Measurements of Dust and Ozone, and (3) Atmospheric Extinction at High Altitudes.

In the study of Atmospheric Motions the magnitude of synoptic accelerations and small scale motions were found to cause almost equal geostrophic departures of the order of 15 to 20% of the geostrophic wind.

The simultaneous dust and ozone profiles show remarkable correspondence in their intermediate scale structure in the region of the lower stratosphere or upper troposphere, the hyopthesis made, therefore, that the source of both constituents lies above the tropopause.

A program to measure solar extinction in the upper atmosphere has only just begun. Extinction is measured in three wavelength regions primarily to determine the dust and ozone concentration at levels above the tropopause. Preliminary analysis of the infrared extinction by relatively large particulate matter shows it to be consistent with the dust distribution and concentration measured directly.

DD FORM 1 JAN 64 1473

Security Classification

Security Classification

14 KEY WORDS	LINK A ROLE	LINK A WT	LINK B ROLE	LINK B WT	LINK C ROLE	LINK C WT
Dust						
Ozone						
Atmospheric Extinction						
Geostrophic Departures						

INSTRUCTIONS

1. ORIGINATING ACTIVITY: Enter the name and address of the contractor, subcontractor, grantee, Department of Defense activity or other organization *(corporate author)* issuing the report.

2a. REPORT SECURITY CLASSIFICATION: Enter the overall security classification of the report. Indicate whether "Restricted Data" is included. Marking is to be in accordance with appropriate security regulations.

2b. GROUP: Automatic downgrading is specified in DoD Directive 5200.10 and Armed Forces Industrial Manual. Enter the group number. Also, when applicable, show that optional markings have been used for Group 3 and Group 4 as authorized.

3. REPORT TITLE: Enter the complete report title in all capital letters. Titles in all cases should be unclassified. If a meaningful title cannot be selected without classification, show title classification in all capitals in parenthesis immediately following the title.

4. DESCRIPTIVE NOTES: If appropriate, enter the type of report, e.g., interim, progress, summary, annual, or final. Give the inclusive dates when a specific reporting period is covered.

5. AUTHOR(S): Enter the name(s) of author(s) as shown on or in the report. Enter last name, first name, middle initial. If military, show rank and branch of service. The name of the principal author is an absolute minimum requirement.

6. REPORT DATE: Enter the date of the report as day, month, year; or month, year. If more than one date appears on the report, use date of publication.

7a. TOTAL NUMBER OF PAGES: The total page count should follow normal pagination procedures, i.e., enter the number of pages containing information.

7b. NUMBER OF REFERENCES: Enter the total number of references cited in the report.

8a. CONTRACT OR GRANT NUMBER: If appropriate, enter the applicable number of the contract or grant under which the report was written.

8b, 8c, & 8d. PROJECT NUMBER: Enter the appropriate military department identification, such as project number, subproject number, system numbers, task number, etc.

9a. ORIGINATOR'S REPORT NUMBER(S): Enter the official report number by which the document will be identified and controlled by the originating activity. This number must be unique to this report.

9b. OTHER REPORT NUMBER(S): If the report has been assigned any other report numbers *(either by the originator or by the sponsor)*, also enter this number(s).

10. AVAILABILITY/LIMITATION NOTICES: Enter any limitations on further dissemination of the report, other than those imposed by security classification, using standard statements such as:

(1) "Qualified requesters may obtain copies of this report from DDC."

(2) "Foreign announcement and dissemination of this report by DDC is not authorized."

(3) "U. S. Government agencies may obtain copies of this report directly from DDC. Other qualified DDC users shall request through _____."

(4) "U. S. military agencies may obtain copies of this report directly from DDC. Other qualified users shall request through _____."

(5) "All distribution of this report is controlled. Qualified DDC users shall request through _____."

If the report has been furnished to the Office of Technical Services, Department of Commerce, for sale to the public, indicate this fact and enter the price, if known.

11. SUPPLEMENTARY NOTES: Use for additional explanatory notes.

12. SPONSORING MILITARY ACTIVITY: Enter the name of the departmental project office or laboratory sponsoring *(paying for)* the research and development. Include address.

13. ABSTRACT: Enter an abstract giving a brief and factual summary of the document indicative of the report, even though it may also appear elsewhere in the body of the technical report. If additional space is required, a continuation sheet shall be attached.

It is highly desirable that the abstract of classified reports be unclassified. Each paragraph of the abstract shall end with an indication of the military security classification of the information in the paragraph, represented as (TS), (S), (C), or (U).

There is no limitation on the length of the abstract. However, the suggested length is from 150 to 225 words.

14. KEY WORDS: Key words are technically meaningful terms or short phrases that characterize a report and may be used as index entries for cataloging the report. Key words must be selected so that no security classification is required. Identifiers, such as equipment model designation, trade name, military project code name, geographic location, may be used as key words but will be followed by an indication of technical context. The assignment of links, rules, and weights is optional.

DD FORM 1473 (BACK)

END